University of California Merced

Asymptotic analysis of boundary integral equations of regions with high curvature

A Thesis submitted in partial satisfaction of the requirements for the degree of Master of Science

in

APPLIED MATHEMATICS

by

LORI LEWIS

Committee in charge:
    Professor Camille Carvalho, Chair
    Professor Arnold D. Kim
    Professor Shilpa Khatri

2020

This is to certify that I have examined a copy of a technical report by

Lori Lewis

and found it satisfactory in all respects, and that any and all revisions required by the examining committee have been made.

Applied Mathematics
Graduate Studies Chair:

_____

Professor Roummel Marcia

Thesis Committee:

_____

Professor Arnold D. Kim

Thesis Committee:

_____

Professor Shilpa Khatri

Committee Chair / Research Advisor:

_____

Professor Camille Carvalho

_____

Date

Contents

List of Symbols

D: domain

B: boundary

f: smooth data

ϵ: perturbation parameter

x: points

y: points

μ: density

K: kernel

N: number of quadrature points

$|y'(s)|$, $|y'(t)|$: Jacobian

t,s: angles

$d\sigma_y$: differential boundary element

$G(x, y)$: Green's function.

$n(s), n(t)$, n_x, n_y: unit outward normal.

C^1 : the space of continuous functions, that are once differentiable.

C^2 : the space of continuous functions, that are twice differentiable.

s_i, t_j: quadrature points on the boundary

Δt: $= \frac{2\pi}{N}$.

$\hat{k}_n$: Fourier coefficients of the kernel.

E: exterior $(\mathbb{R}^2 \setminus \bar{D})$.

k: wavenumber associated with the source.

i: imaginary number.

$H_0^{(1)}$, $H_1^{(1)}$: Hankel function of the first kind.

C: Euler's constant.

PTR: Periodic Trapezoid Rule

MTR: Modified Trapezoid Rule

I: identity matrix

P: matrix obtained from the discretization of the double-layer potential using PTR for the interior Dirichlet problem.

M: matrix obtained from the discretization of the double-layer potential using MTR for the interior Dirichlet problem.

A: matrix obtained from the Fourier Series coefficients for the interior Dirichlet problem.

P_E: matrix obtained from the discretization of the adjoint double-layer potential using PTR for the exterior Neumann problem.

M_E: matrix obtained from the discretization of the adjoint double-layer potential using MTR for the exterior Neumann problem.

H: matrix obtained from the discretization of the single and double-layer potentials using Kress quadrature for the exterior Helmholtz problem.

List of Figures

Acknowledgements

First and foremost, I thank my advisor Dr. Camille Carvalho. Professor Carvalho has shared her mathematical expertise to help me in my research and has devoted time to my mathematical education without her this thesis would not be possible. I would also like to thank my committee members, Dr. Arnold Kim and Dr. Shilpa Khatri, for reading my thesis and offering suggestions. In particular I thank Professor Kim for serving as a co- advisor and for his advice concerning the first result of this thesis.

I would also like to thank my fellow math graduate students. Whenever I needed advice about math concepts or had questions about graduate life, they were there for me.

Last but not least, I would like to thank my friends. From whose conversations and support provided a balance to the world of math and helped me keep my sanity.

Thank you all for all your support!

Asymptotic analysis of boundary integral equations of regions with high curvature

by

Lori Lewis

Master of Science in Applied Mathematics

Dr. Camille Carvalho, Committee Chair

University of California, Merced

2020

Abstract

In this project we investigate the behavior of layer potentials in regions of high curvature in two dimensions, in particular an asymptotically collapsing ellipse. Layer potentials arise in boundary integral methods and offer several advantages numerically but can be affected by regions of high curvature. Such phenomena appear in slender body theory. In this thesis we propose two approaches to address this challenge. We propose a modification of quadrature rules using asymptotic methods, and a spectral method when one can find the analytic Fourier coefficients. We apply these techniques to several problems: Laplace's problems (interior Dirichlet and exterior Neumann), and a scattering problem.

Chapter 1

Introduction

Boundary integral equation (BIE) methods can be used to solve elliptic boundary value problems based on partial differential equations [13, 22, 18]. The solution to a boundary value problem is then represented as a layer potential, an integral over the boundary involving a kernel (related to the fundamental solution of the elliptic PDE at stake) and a continuous density related to the boundary value problem's data. Boundary integral methods are advantageous methods: they allow us to reduce the problem by one dimension, and solutions of boundary value problems can be approximated using high order numerical methods [26, 14, 16, 20, 10, 7, 19]. However, BIE methods often lead to working with dense matrices which can be costly to invert.

Boundary integral methods are commonly used in electromagnetism [15], and fluid dynamics [21, 23]. An important component of these applications is that it is important to compute accurately the field (electromagnetic, fluid velocity, etc.) close to the boundary. Such evaluations are required for applications such as deformable drops in Stokes flow, and holography of colloids and droplets [21, 27].

One of the challenges of BIE method is the close evaluation problem [13, 14]. This refers to large errors occurring due to approximating nearly singular integrals: the integrals of nearly singular kernels exhibits a peaked behavior which is then under-resolved numerically. BIE methods can present weakly singular integrals, and/ or nearly singular integrals. There exist high-order quadrature rules to approximate weakly singular integrals [14, 10, 16, 20, 26, 7, 19]. Nearly singular integrals are more challenging [25, 3]. Recent work [5, 6] provides techniques to efficiently approximate nearly singular integrals such as using asymptotics to characterize the nearly singular behavior, or using spectral methods when the integrand can be written as a rational trigonometric function.

Motivated by slender body theory [24], in this thesis we investigate BIE with regions of high curvature. Regions of high curvature yield nearly singular behaviors which affect the accuracy of standard numerical methods. We propose to address this challenge by using asymptotic and spectral methods. In particular we provide 2 techniques: a local correction to standard quadrature rules using an inner asymptotic expansion of the integrand [11, 5], and a spectral method based on Fourier Series [7]. We focus on investigating 3 problems in two dimensions: the

interior Dirichlet Laplace (Chapter 2), the exterior Neumann Laplace (Chapter 3), and the exterior Helmholtz problem (Chapter 4). Chapter 5 presents our concluding remarks. The appendices provide additional results: appendix A gives a proof of the representation formula, appendices B, D, and E detail calculations for the inner asymptotic expansion for the Laplace problems and scattering problem, appendix C details additional calculations used in Chapter 3, appendix F presents calculations for the matched asymptotics for the interior Dirichlet Laplace problem. Finally, appendices G and H detail results using a body-fitted grid for the exterior Neumann Laplace and exterior Helmholtz problems.

Chapter 2

Interior Dirichlet Laplace

We study Laplace's equation in a domain whose boundary has regions of high curvature, in particular, a narrow ellipse. We consider here a specific problem for which we know the solution using Gauss Law [25]. We seek to find $u \in C^2(D) \cup C^1(\bar{D})$ satisfying

$$\Delta u = 0 \quad \text{in} \quad D,$$
$$u = f \quad \text{on} \quad B. \tag{2.1}$$

Here D is an elliptical domain, B is the boundary and f is a smooth data (source).
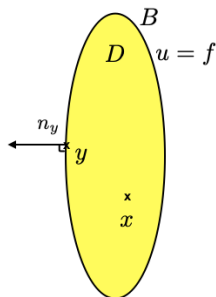
Figure 2.1: Ellipse for the Interior Dirichlet Laplace problem (2.1). Here x is a point in D, y is a point on B and n_y is the unit outward normal at y.

It is well known that the solution of problem (2.1) can be represented as the double-layer potential [13],

$$u(x) = \int_B \frac{\partial G}{\partial n_y}(x,y)\mu(y)\mathrm{d}\sigma_y, \quad x \in D, \tag{2.2}$$

where n_y is the unit outward normal at y, and $\mathrm{d}\sigma_y$ is the differential boundary element. In (2.2), $G(x,y)$ denotes Green's function for Laplace's equation,

$$G(x,y) = -\frac{1}{2\pi}\log|x-y|, \tag{2.3}$$

and μ is the continuous density function that satisfies the following Boundary Integral Equation (BIE),

$$-\frac{1}{2}\mu(x) + \int_B \frac{\partial G}{\partial n_y}(x,y)\mu(y)\mathrm{d}\sigma_y = f(x), \quad x \in B, \tag{2.4}$$

where $\quad \dfrac{\partial G}{\partial n_y}(x, y) = \dfrac{1}{2\pi} n_y \cdot \dfrac{x - y}{|x - y|^2}.$

Note, in the BIE x lies on the boundary.

2.1   Parameterization

We are interested in solving (2.1) accurately and studying the effect of the curvature on its accuracy. We make use of explicit parameterization $y = y(t) = \langle y_1(t), y_2(t) \rangle$ where $0 \leq t \leq 2\pi$. For the BIE, we write $x \in B$, $x = y(s)$ for $s \in [0, 2\pi]$, $\mu(y(t)) = \mu(t)$ and $f(x) = f(s)$. The BIE then becomes

$$-\frac{1}{2}\mu(s) + \frac{1}{2\pi} \int_0^{2\pi} n(t) \cdot \frac{y(s) - y(t)}{|y(s) - y(t)|^2} |y'(t)| \mu(t) \mathrm{d}t = f(s), \quad 0 \leq s \leq 2\pi, \quad (2.5)$$

where $n_y = n(y(t)) = n(t)$ is the unit outward normal, and $|y'(t)|$ is the Jacobian.

The kernel of the double-layer potential in (2.5) is given by

$$K(s, t) = n(t) \cdot \frac{y(s) - y(t)}{|y(s) - y(t)|^2} |y'(t)|. \quad (2.6)$$

To describe the ellipse, we introduce the parameterization,

$$y(t) = \langle \epsilon \cos(t), \sin(t) \rangle, \quad 0 \leq t \leq 2\pi. \quad (2.7)$$

The outward normal vector is

$$n(t) = \frac{\langle \cos(t), \epsilon \sin(t) \rangle}{|y'(t)|} = \frac{\langle \cos(t), \epsilon \sin(t) \rangle}{\sqrt{\epsilon^2 \sin^2(t) + \cos^2(t)}}. \quad (2.8)$$

We rewrite (2.6) and find that

$$K(s, t; \epsilon) = \frac{\langle \cos(t), \epsilon \sin(t) \rangle}{|y'(t)|} \cdot \frac{y(s) - y(t)}{|y(s) - y(t)|^2} |y'(t)| \quad (2.9)$$

$$= \frac{\epsilon}{-1 - \epsilon^2 - (1 - \epsilon^2) \cos(s + t)}. \quad (2.10)$$

The above expression is exact and, $K(s, t; \epsilon)$ is nearly singular [25] when $s + t = \pi$ or $s + t = 3\pi$ since $\cos(s + t) = -1$ then

$$K(s, t; \epsilon) = -\frac{1}{2\epsilon}.$$

It follows that

$$\lim_{\epsilon \to 0} K(s, t; \epsilon) \to -\infty.$$

Figure 2.2 shows the behavior of the kernel with different values of ϵ. When $s + t = \pi$ the kernel has a sharp peak. Although it is not shown in Figure 2.2, the same peaked behavior appears for $s + t = 3\pi$. We notice that as $\epsilon \to 0$ the peak becomes more prominent. Such behavior makes the Boundary Integral Equation,

4

$$-\frac{1}{2}\mu(s) + \frac{1}{2\pi}\int_0^{2\pi} \frac{\epsilon}{-1-\epsilon^2-(1-\epsilon^2)\cos(s+t)}\mu(t)\mathrm{d}t = f(s), \quad 0 \le s \le 2\pi, \tag{2.11}$$

hard to solve with numericcal methods.
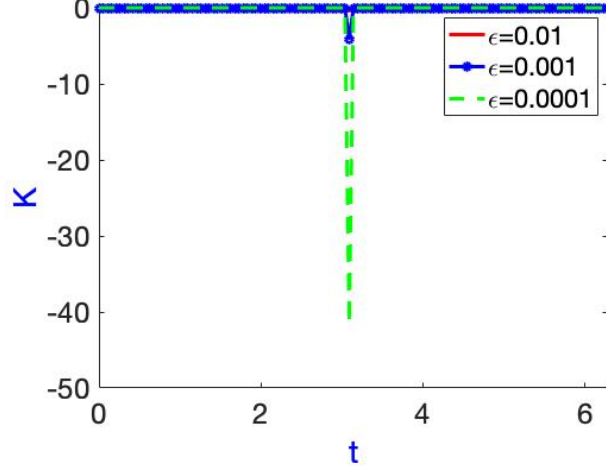
Figure 2.2: Plots showing the behavior of the kernel for a fixed $s = \frac{\pi}{16}$ with various values of ϵ.

2.2 Numerical Investigation

We use a quadrature method to discretize the BIE (2.11), in particular with the Periodic Trapezoid Rule (PTR). We start by setting N equally spaced quadrature points on $0 \le t \le 2\pi$. The boundary integral equation (2.11) when using the Periodic Trapezoid Rule then becomes

$$-\frac{1}{2}\mu(s_i) + \frac{1}{N}\sum_{j=1}^{N} K(s_i, t_j; \epsilon)\mu(t_j) = f(s_i), \quad i = 1, \ldots, N. \tag{2.12}$$

Here $s_i = \frac{(2\pi)i}{N}$ and $t_j = \frac{(2\pi)j}{N}$ $i, j = 1, \ldots, N$. The Periodic Trapezoid Rule is used to compute an approximation of the density μ to the BIE (2.11). To obtain this approximation, we solve the system,

$$\left(-\frac{1}{2}I_N + P\right)\mu_N = f_N, \tag{2.13}$$

where P is the matrix obtained from the discretization of the double-layer potential on B discretized using the Periodic Trapezoid Rule (2.12). Here μ_N and f_N represent the discretization of μ and f at the quadrature points.

To investigate the effect of ϵ using the method, we compare the approximation with an exact solution and study the error. To obtain an exact solution, we use Gauss' law [25] for the double-layer potential,

$$\int_B \frac{\partial G}{\partial n_y}(x,y)\mathrm{d}\sigma_y = \begin{cases} -1, & x \in D \\ -\frac{1}{2}, & x \in B \\ 0, & x \in E \end{cases} \tag{2.14}$$

If we assume μ to be constant $(\mu = \mu_o)$ then the BIE gives us

$$-\frac{1}{2}\mu_o + \frac{1}{2\pi}\int_0^{2\pi} K(s,t;\epsilon)\mu_o\mathrm{d}t = f(s), \quad 0 \leq s \leq 2\pi.$$

Using Gauss' Law, we find

$$-\frac{1}{2}\mu_o - \frac{1}{2}\mu_o = -\mu_o = f(s), \quad 0 \leq s \leq 2\pi \tag{2.15}$$

is satisfied if $f(s) = -\mu_o$. We choose $f = 1$, so that $\mu_o = -1$. Using $f = 1$, we compare the approximations obtained numerically to the exact solution $\mu = -1$.

2.3 Numerical Results

Figure 2.3a shows the approximation of μ for different values of ϵ using PTR. As $\epsilon \to 0$, the error of the approximation grows. The approximation overestimates the exact solution, $\mu = -1$. Figure 2.3b shows a log-log plot of the error versus N in which it can be observed error decreases as N increases. The error is O (1) for PTR and it does not do a good job capturing the peak of the kernel. Recall that the kernel $K(s,t;\epsilon)$ is nearly singular when $s + t = \pi$ or $s + t = 3\pi$ which corresponds to the anti-diagonals observed in the heatmap of the PTR matrix P in Figure 2.4. We computed the condition number of the matrix $(-\frac{1}{2}I_N + P)$ to be $85,56055$. We notice that the condition number is much bigger than 1 which means the matrix $(-\frac{1}{2}I_N + P)$ is sensitive to the inverse calculation. Our focus is on the accuracy of the solution rather than cost of inverting a matrix. Since the kernel is nearly singular, it is challenging to solve the boundary integral equation accurately.

(a)   (b)
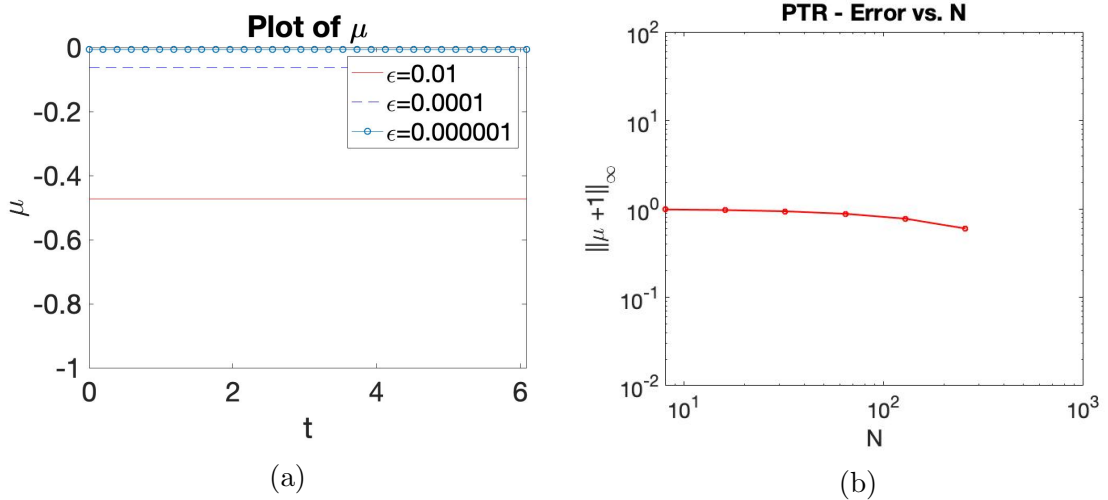
Figure 2.3: (a) The Periodic Trapezoid Rule approximation of μ for different values of ϵ and a fixed $N = 32$. (b) A log-log plot of the error vs. N for the PTR with $\epsilon = 0.001$.

(a)
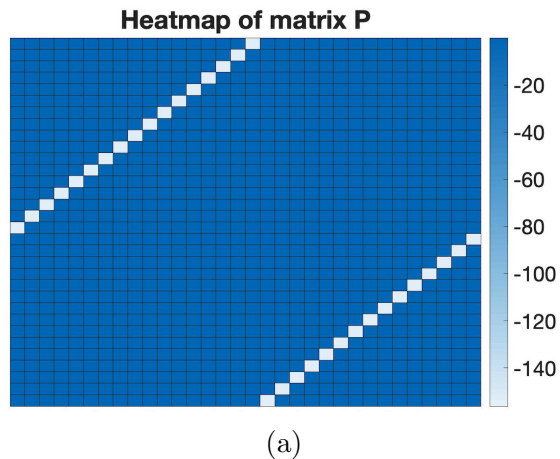
Figure 2.4: Heatmap of the matrix P given in (2.13).

2.4 Inner Asymptotic Expansion

We seek to improve the approximation of the Periodic Trapezoid Rule by performing an asymptotic approximation where the kernel is nearly singular, i.e. $s+t = \pi$ and $s + t = 3\pi$. We start by looking at the integral of the boundary integral equation

$$I = \int_0^{2\pi} K(s, t; \epsilon)\mu(t)\mathrm{d}t. \tag{2.16}$$

We evaluate the integral at a neighborhood around the point $y(t) = y(\pi - s)$, where we seek to introduce an inner asymptotic expansion. On the boundary both angles $s + t = \pi$ and $s + t = 3\pi$ correspond to the same point on the ellipse. Thus we can use the approximation we get about $y(t) = y(\pi - s)$ for both points, as seen in Figure 2.5.

7
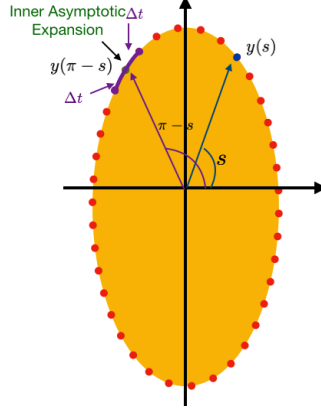
Figure 2.5: Neighborhood around point $y(\pi - s)$ on the ellipse where we seek to determine the inner asymptotic expansion.

We consider the interval $[\pi - s - \Delta t, \pi - s + \Delta t]$, and the integral

$$I_1 = \int_{\pi-s-\Delta t}^{\pi-s+\Delta t} K(s,t;\epsilon)\mu(t)\mathrm{d}t \tag{2.17}$$

where $\Delta t = \frac{2\pi}{N}$ is fixed.

To obtain an inner asymptotic expansion for I_1 we do a series of substitutions. We shift by substituting $t = \tau + \pi - s$ with $\mathrm{d}t = \mathrm{d}\tau$ leading to

$$I_1 = \frac{1}{2\pi}\int_{-\Delta t}^{\Delta t} K(s, \tau + \pi - s; \epsilon)\mu(\tau + \pi - s)\mathrm{d}\tau. \tag{2.18}$$

Next, we scale by ϵ according to $\tau = \epsilon T$ with $\mathrm{d}\tau = \epsilon\mathrm{d}T$ and obtain

$$I_1 = \frac{1}{2\pi}\int_{-\frac{\Delta t}{\epsilon}}^{\frac{\Delta t}{\epsilon}} K(s, \epsilon T + \pi - s; \epsilon)\mu(\epsilon T + \pi - s)\epsilon\mathrm{d}T. \tag{2.19}$$

Using Mathematica (Appendix B), we expand the kernel K and the density μ in (2.19) about $\epsilon = 0$ to obtain

$$K(s, \epsilon T + \pi - s; \epsilon) = \frac{1}{(-2 - \frac{T^2}{2})\epsilon} + \frac{(-12T^2 - T^4)\epsilon}{6(4 + T^2)^2} + O(\epsilon^3), \tag{2.20}$$

$$\mu(\epsilon T + \pi - s) = \mu(\pi - s) + \epsilon T\mu(\pi - s) + O(\epsilon^2). \tag{2.21}$$

Because we scale by ϵ, we integrate the leading order terms of the expansion and find that

$$I_1 = \frac{1}{2\pi}\int_{-\frac{\Delta t}{\epsilon}}^{\frac{\Delta t}{\epsilon}} \frac{\mu(\pi - s)}{\left(-2 - \frac{T^2}{2}\right)\epsilon}\epsilon\mathrm{d}T + O(\epsilon) = -\frac{\arctan(\frac{\Delta t}{2\epsilon})\mu(\pi - s)}{\pi} + O(\epsilon). \tag{2.22}$$

At the points where the nearly singular behavior happens, $y(s + t) = y(\pi)$ and $y(s + t) = y(3\pi)$, we replace PTR with the inner asymptotic expansion given in (2.22). For all other points we use the Composite Trapezoid Rule to obtain an

approximation for μ. We call this method the Modified Trapezoid Rule (MTR), and when applied to (2.11) yields

$$-\frac{1}{2}\mu(s_i)+\frac{1}{N}\sum_{\substack{j=1\\s_i+t_j\neq\pi\\s_i+t_j\neq 3\pi}}^{N} K(s_i,t_j;\epsilon)\mu(t_j)+\sum_{\substack{s_i+t_j=\pi\\s_i+t_j=3\pi}}\left(-\frac{\arctan(\frac{\Delta t}{2\epsilon})\mu(\pi-s)}{\pi}\right) = f(s_i),$$

$$i=1,\ldots,N$$

(2.23)

We use the MTR to obtain an approximation of the BIE (2.11) by solving the system,

$$\left(-\frac{1}{2}I_N+M\right)\mu_N = f_N,$$

(2.24)

where M is the matrix obtained from the discretization of the double-layer potential on B obtained using the Modified Trapezoid Rule.

2.5 Numerical Results

We use the exact solution for $f=1$ given by $\mu=-1$ to verify our approximation obtained for MTR. Figure 2.6a shows the approximations of μ by MTR for $\epsilon = 10^{-2}$, 10^{-4}, and 10^{-6}. MTR is accurate because it makes a correction on the points where the kernel is nearly singular. Figure 2.6b shows the heatmap of the matrix M in (2.24). The correction of the inner asymptotic expansion along the anti-diagonals $s+t=\pi$ and $s+t=3\pi$ leads to much smaller values since it accounts for the nearly singular behavior. We notice that the condition number of matrix $(-\frac{1}{2}I+M)$ is 1.064731. The condition number is much closer to 1 which means there is no problem solving (2.24). Here we notice that the conditioned number of $(-\frac{1}{2}I_N+M)$ is better than the condition number of matrix $(-\frac{1}{2}I_N+P)$. Recall that we focus on the accuracy of the solution rather than cost of inverting the matrix. Figure 2.7a contains the log-log plot of the error with respect to ϵ. It can be observed that as ϵ decreases, the error decreases for the MTR. In contrast the error of PTR increases as ϵ decreases. Considering we are interested in studying the regions of high curvature, we focus on the error as ϵ gets smaller. The error plots in Figure 2.7b, shows the errors for both PTR and MTR with respect to N. MTR requires fewer discretization points to obtain an accurate approximation because of the correction made on the points where the kernel is nearly singular.

We can see from Figure 2.7a as $\epsilon \to 0$ MTR approximation is more accurate than PTR approximation. We notice that the error for MTR increases and the error for PTR decreases. MTR is $O(\epsilon)$ and the error grows linearly with ϵ. For a large enough ϵ, PTR achieves spectral convergence. We can observe from Figure 2.7b that MTR requires very few points to obtain an approximation of μ. MTR provides an efficient local correction to improve PTR from approximating the BIE (2.11). In the next sections we seek for an alternative method to recover spectral accuracy.
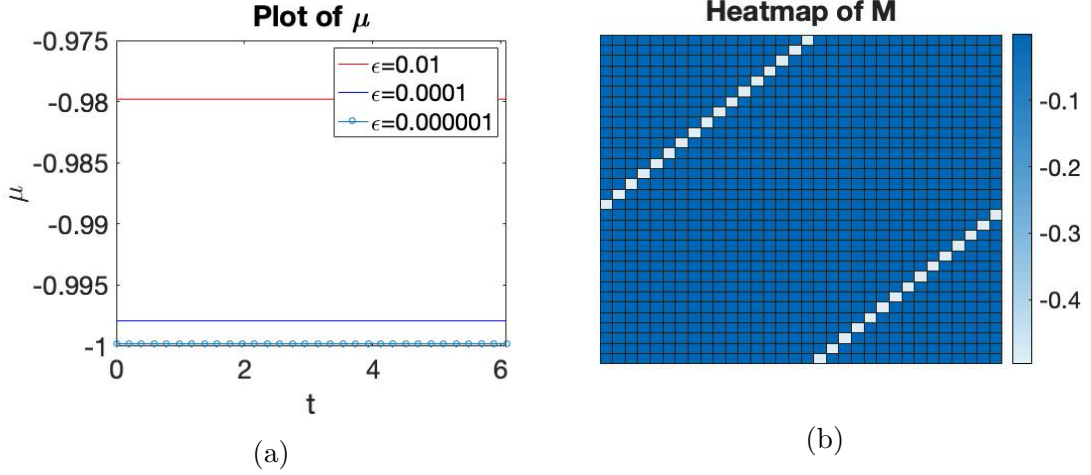
Figure 2.6: (a) The approximation μ using the Modified Trapezoid Rule (MTR) with $N = 32$ and $\epsilon = 10^{-2}$, 10^{-4}, and 10^{-6}. (b) Heatmap of the MTR matrix.
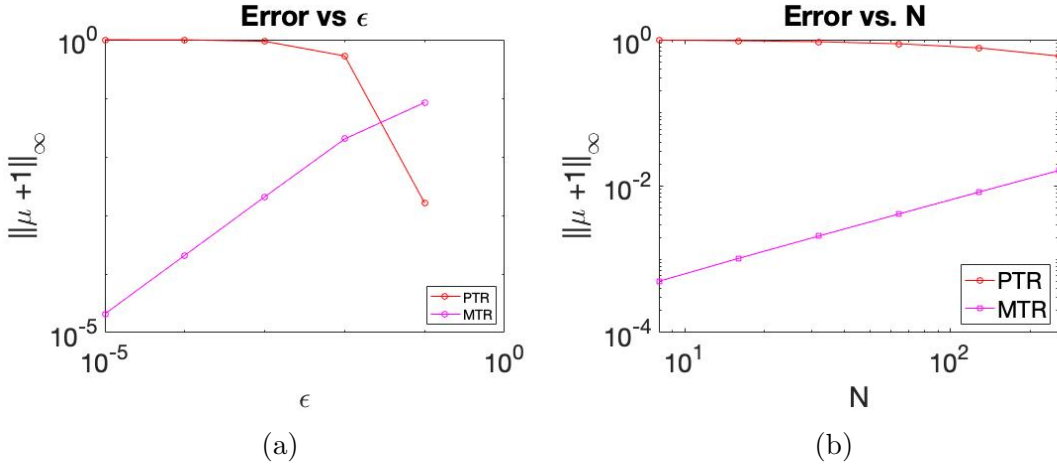
Figure 2.7: (a) Log-log plot of the error with respect to ϵ for $N = 32$. (b) Log-log plot of the error with respect to N with $\epsilon = 0.001$.

2.6 Spectral Method

Since we have a closed curve and periodic functions, we are able to use a Fourier spectral method as an alternative approach. The Fourier series provides a direct method to solve the Boundary Integral Equation. Recall that the BIE we are solving is

$$-\frac{1}{2}\mu(s) + \frac{1}{2\pi}\int_0^{2\pi} K(s,t;\epsilon)\mu(t)\mathrm{d}t = f(s) \quad s \in [0, 2\pi] \tag{2.25}$$

We represent the unknown $\mu(s)$ with its Fourier series

$$\mu(s) = \sum_{n=-\infty}^{\infty} \hat{\mu}_n e^{ins}, \quad \text{where} \quad \hat{\mu}_n = \frac{1}{2\pi}\int_0^{2\pi} \mu(s)e^{-ins}\mathrm{d}s, \tag{2.26}$$

and write $f(s) = \sum_{n=-\infty}^{\infty} \hat{f}_n e^{-ins}$, with $\hat{f}_n = \frac{1}{2\pi} \int_0^{2\pi} f(s) e^{-ins} \mathrm{d}s$.

We derive an equation for $\hat{\mu}_n$ for $n = -\infty, \ldots, \infty$. By multiplying the BIE (2.25) by $\frac{1}{2\pi} e^{-ins}$ and integrating with respect to s we get

$$-\frac{1}{2} \frac{1}{2\pi} \int_0^{2\pi} e^{-ins} \mu(s) \mathrm{d}s + \frac{1}{2\pi} \int_0^{2\pi} \left[\frac{1}{2\pi} \int_0^{2\pi} K(s,t;\epsilon) e^{-ins} \mu(t) \mathrm{d}t \right] \mathrm{d}s$$
$$= \frac{1}{2\pi} \int_0^{2\pi} e^{-ins} f(s) \mathrm{d}s, \quad (2.27)$$

leading to

$$-\frac{1}{2} \hat{\mu}_n + \frac{1}{2\pi} \int_0^{2\pi} \left[\frac{1}{2\pi} \int_0^{2\pi} K(s,t;\epsilon) e^{-ins} \mu(t) \mathrm{d}t \right] \mathrm{d}s = \hat{f}_n. \quad (2.28)$$

Now we substitute

$$\mu(t) = \sum_{n'=-\infty}^{\infty} \hat{\mu}_{n'} e^{in't} \quad (2.29)$$

into (2.28) and find

$$-\frac{1}{2} \hat{\mu}_n + \sum_{n'=-\infty}^{\infty} \hat{\mu}_{n'} \left[\frac{1}{2\pi} \int_0^{2\pi} \frac{1}{2\pi} \int_0^{2\pi} K(s,t;\epsilon) e^{-ins} e^{in't} \mathrm{d}t \mathrm{d}s \right] = \hat{f}_n. \quad (2.30)$$

Let us define

$$\hat{k}_{nn'} = \frac{1}{2\pi} \int_0^{2\pi} \frac{1}{2\pi} \int_0^{2\pi} K(s,t;\epsilon) e^{-ins} e^{in't} \mathrm{d}t \mathrm{d}s, \quad n, n' \in \mathbb{N}. \quad (2.31)$$

Then (2.30) simplifies to

$$-\frac{1}{2} \hat{\mu}_n + \sum_{n'=-\infty}^{\infty} \hat{\mu}_{n'} \hat{k}_{nn'} = \hat{f}_n. \quad (2.32)$$

If $\hat{k}_{nn'}$ and $\hat{f}_n$ are known then we can solve for $\hat{\mu}_n$. We investigate the expression of $\hat{k}_{nn'}$ in our case. We begin by looking at the kernel

$$K(s,t;\epsilon) = \frac{\epsilon}{-1 - \epsilon^2 - (1 - \epsilon^2) \cos(s+t)}.$$

Since K depends only on $s + t$ we can assume that

$$K(s,t;\epsilon) = \sum_{m=-\infty}^{\infty} \hat{k}_m e^{im(s+t)}. \quad (2.33)$$

Then $\hat{k}_{nn'}$ becomes, using equation (2.31) and (2.33)

$$\hat{k}_{nn'} = \frac{1}{2\pi} \int_0^{2\pi} \frac{1}{2\pi} \int_0^{2\pi} \sum_{m=-\infty}^{\infty} \hat{k}_m e^{im(s+t)} e^{-ins} e^{in't} \mathrm{d}t \mathrm{d}s$$

$$= \sum_{m=-\infty}^{\infty} \hat{k}_m \left(\frac{1}{2\pi} \int_0^{2\pi} e^{i(m-n)s} \mathrm{d}s \right) \left(\frac{1}{2\pi} \int_0^{2\pi} e^{i(m+n')t} \mathrm{d}t \right). \qquad (2.34)$$

Note that

$$\frac{1}{2\pi} \int_0^{2\pi} e^{i(m-n)s} \mathrm{d}s = \frac{1}{2\pi} \frac{1}{i(m-n)} \left[e^{i(m-n)s} \right]_0^{2\pi}$$

$$= \frac{1}{2\pi} \frac{1}{i(m-n)} (e^{i(m-n)2\pi} - 1)$$

$$= \begin{cases} 1, & m-n=0 \\ 0, & m-n \neq 0. \end{cases} \qquad (2.35)$$

Similarly,

$$\frac{1}{2\pi} \int_0^{2\pi} e^{i(m+n')t} \mathrm{d}t = \begin{cases} 1, & m+n'=0 \\ 0, & m+n' \neq 0. \end{cases} \qquad (2.36)$$

Now that we have evaluated the integrals we find $\hat{k}_{nn'} = k_{nn} = \hat{k}_n$. We can include these coefficients into the BIE to obtain

$$-\frac{1}{2} \hat{\mu}_n + \hat{\mu}_{-n} \hat{k}_n = \hat{f}_n, \quad n = -\infty, \dots, \infty \qquad (2.37)$$

To be able to solve for $\hat{\mu}_n$ we need to find the Fourier coefficient of the kernel, $\hat{k}_n$.

2.6.1 Finding the Fourier Series coefficients of the kernel

Since $K(s,t;\epsilon)$ is a rational trigonometric function there exist results [12] which allow us to find analytically the Fourier coefficients of a rational trigonometric function. We will use this technique to find the coefficients of the kernel (2.10),

$$K(s,t;\epsilon) = \left(\frac{-\epsilon}{1+\epsilon^2} \right) \left(\frac{1}{1 + \frac{1-\epsilon^2}{1+\epsilon^2} \cos(s+t)} \right) = \left(\frac{c_0}{1 + c_1 \cos(s+t)} \right), \qquad (2.38)$$

with $c_0 = \frac{-\epsilon}{1+\epsilon^2}$ and $c_1 = \frac{1-\epsilon^2}{1+\epsilon^2}$. Note that $0 < c_1 < 1$ for $0 < \epsilon < 1$.

Let $x = s + t$. According to Geer [12], we can find the Fourier coefficients $\hat{k}_m$ as follows

$$\hat{k}_m = \frac{1}{2\pi} \int_{-\pi}^{\pi} K(x;\epsilon) e^{-im(x)} \mathrm{d}x \qquad (2.39)$$

12

$$= \frac{1}{2\pi} \int_{-\pi}^{\pi} \frac{c_0}{1 + c_1 \cos(x)} \left(\cos(mx) - i \sin(mx) \right) \mathrm{d}x$$

$$= \frac{1}{2\pi} \int_{-\pi}^{\pi} \frac{c_0}{1 + c_1 \cos(x)} \cos(mx) \mathrm{d}x$$

$$= \frac{c_0}{\pi} \int_0^{\pi} \frac{1}{1 + c_1 \cos(x)} \cos(mx) \mathrm{d}x$$

$$= c_0 I_{m,1} \quad \text{where} \quad I_{m,1} = \rho^m \frac{1 + \rho^2}{1 - \rho^2} \quad \text{for} m \geq 0, \quad \text{and} \quad \rho = \frac{\sqrt{1 - c_1^2} - 1}{c_1}.$$

We obtain

$$\hat{k}_m = c_0 \frac{1 + \rho^2}{1 - \rho^2} \rho^{|m|}, \quad \forall m \in \mathbb{N}. \tag{2.40}$$

Plugging these coefficients into (2.37) and truncating the system to include only N terms, we obtain

$$-\frac{1}{2}\hat{\mu}_n + \hat{\mu}_{-n}\hat{k}_n = \hat{f}_n, \quad n = -\frac{N}{2}, \dots, \frac{N}{2} - 1. \tag{2.41}$$

Equation (2.41) is a linear system which can be written as follows

$$\begin{bmatrix} -\frac{1}{2} & 0 & & \cdots & & 0 \\ 0 & \ddots & & & \iddots & \hat{k}_{\frac{N}{2}-1} \\ & & \ddots & & \iddots & 0 \\ \vdots & & & -\frac{1}{2} + \hat{k}_0 & & \vdots \\ & \iddots & \iddots & & \ddots & 0 \\ 0 & \hat{k}_{-\frac{N}{2}} & 0 & \cdots & 0 & -\frac{1}{2} \end{bmatrix} \begin{bmatrix} \hat{\mu}_{-\frac{N}{2}} \\ \vdots \\ \vdots \\ \hat{\mu}_{\frac{N}{2}-1} \end{bmatrix} = \begin{bmatrix} \hat{f}_{-\frac{N}{2}} \\ \vdots \\ \vdots \\ \hat{f}_{\frac{N}{2}-1} \end{bmatrix}.$$

We solve the system such that

$$A\hat{\mu}_N = \hat{f}_N \tag{2.42}$$

where A is the matrix given above. The system is then solved for $\hat{\mu}_N$ and then we use inverse FFT to find μ.

Figure 2.8a shows the resulting density, μ, for different values of ϵ. The resulting μ using the Fourier series approximates the exact solution as $\epsilon \to 0$. One of the conditions of obtaining the Fourier coefficients is that $c_1 < 1$. Using the expression for c_1, we notice that as $\epsilon \to 0$ we get that $c_1 \to 1$ which means the Spectral method requires N to be larger to obtain good accuracy. Figure 2.8b shows a log-log plot of the error. As $\epsilon \to 0$ the error increases. This is due to the condition on c_1. Although the spectral method is affected by the curvature, it is more accurate than PTR and MTR. The Fourier series provides an accurate approximation for our problem but is limited to a rational trigonometric kernel.
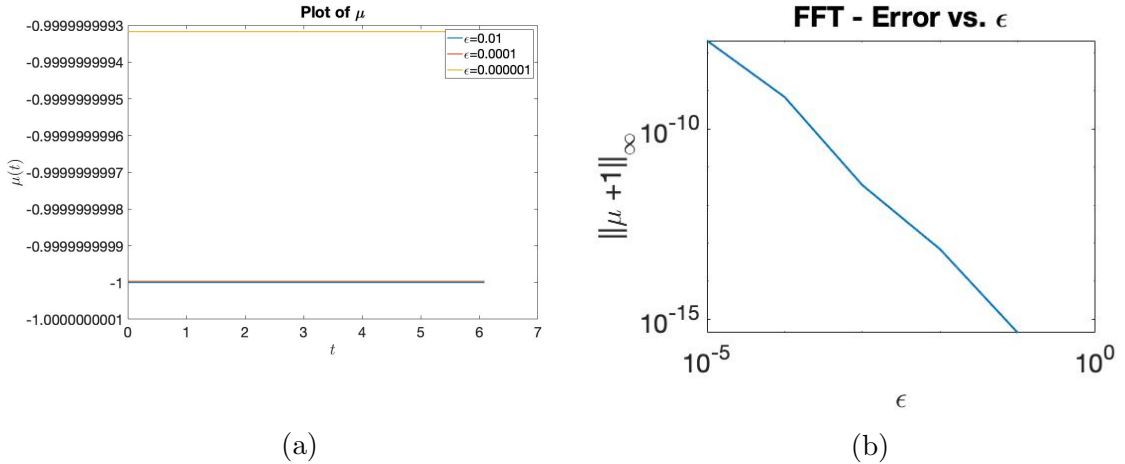
Figure 2.8: (a) The approximate μ using the Spectral method with $N = 32$ and $\epsilon = 10^{-2}$, 10^{-4}, and 10^{-6}. (b) Log-log plot of the error as ϵ is varied and $N = 32$.

2.7 Comparison and Conclusion

In our results, we found that for $N = 32$ and $\epsilon = 0.1$, the Spectral method has 15 digits of accuracy, PTR has a $O(1)$ error, and MTR has 4 digits of accuracy. Although the Spectral method is more accurate than MTR and PTR, it is limited to a rational trigonometric kernel. We were able to use a Fourier series approximation because the kernel to our problem has an explicit form so that the Fourier coefficients were accessible. The PTR approximation was inaccurate but does not restrict to a specific kernel and boundary curve. The method we propose, MTR offers accuracy and can be applied to other problems, and other boundary curves. MTR focuses on providing a correction where the kernel is nearly singular through the use of an inner asymptotic expansion. We expanded on matched asymptotics for this problem but confronted complications since one of the integrals blows up (Appendix F). In the following chapters, we use a similar technique as MTR to solve the exterior Neumann Laplace problem and a scattering problem (see Chapters 3 and 4).

Chapter 3

Exterior Neumann Laplace

We study the exterior Neumann Laplace problem in a domain whose boundary has regions of high curvature. We seek to find $u \in C^2(E) \cup C^1(\bar{E})$ satisfying

$$\Delta u = 0, \quad x \in E,$$
$$\frac{\partial u}{\partial n_x} = f, \quad x \in B. \tag{3.1}$$

Here $E := \mathbb{R}^2 \setminus \bar{D}$ is the exterior and B is the boundary represented in Figure 3.1. E is an unbounded domain.
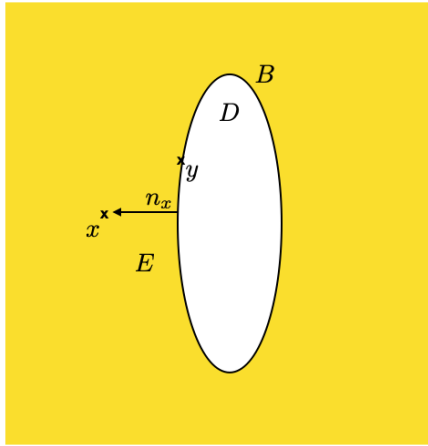
Figure 3.1: Ellipse and notations for the exterior Neumann Laplace problem.

The solution to problem (3.1) can be represented as the single-layer potential,

$$u(x) = \int_B G(x,y)\mu(y)\mathrm{d}\sigma_y, \quad x \in E, \tag{3.2}$$

where the Green's function $G(x,y)$ is given by

$$G(x,y) = -\frac{1}{2\pi}\log|x-y|, \tag{3.3}$$

and $\mu(y)$ is a continuous density that satisfies the following Boundary Integral Equation (BIE),

$$\frac{1}{2}\mu(x) - \int_B \frac{\partial G}{\partial n_x}\mu(y)\mathrm{d}\sigma_y = f(x), \quad x \in B, \tag{3.4}$$

where $\dfrac{\partial G}{\partial n_x} = -\dfrac{1}{2\pi} n_x \cdot \nabla_x(\log|x - y|) = -\dfrac{1}{2\pi} n_x \cdot \dfrac{x - y}{|x - y|^2}.$

Substituting this expression into the BIE, we obtain

$$\frac{1}{2}\mu(x) + \frac{1}{2\pi}\int_B n_x \cdot \frac{x - y}{|x - y|^2}\mu(y)\mathrm{d}\sigma_y = f(x), \quad x \in B. \tag{3.5}$$

3.1 Parameterization

We aim to solve (3.5) accurately and study the effect of the curvature on its accuracy. We make use of explicit parameterization $y = y(t) = \langle y_1(t), y_2(t) \rangle$ where $0 \leq t \leq 2\pi$. For the BIE, $x \in B$, $x = y(s)$ for $s \in [0, 2\pi]$, $\mu(y(t)) = \mu(t)$ and $f(x) = f(s)$. The BIE then becomes

$$\frac{1}{2}\mu(s) + \frac{1}{2\pi}\int_0^{2\pi} n(s) \cdot \frac{y(s) - y(t)}{|y(s) - y(t)|^2}|y'(t)|\mu(t)\mathrm{d}t = f(s), \quad 0 \leq s \leq 2\pi, \tag{3.6}$$

where $n_x = n(y(s)) = n(s)$ and $|y'(t)|$ is the Jacobian.
After plugging in the parameterization for the ellipse, we determine the kernel of the integral operator in (3.6) to be

$$K(s, t; \epsilon) = \frac{\langle \cos s, \epsilon \sin s \rangle}{|y'(s)|} \cdot \frac{y(s) - y(t)}{|y(s) - y(t)|^2}|y'(t)| \tag{3.7}$$

$$= -\frac{\epsilon\sqrt{1 + \epsilon^2 - (-1 + \epsilon^2)\cos(2t)}}{\sqrt{2}(-1 - \epsilon^2 + (-1 + \epsilon^2)\cos(s + t))\sqrt{\cos^2(s) + \epsilon^2\sin^2(s)}}. \tag{3.8}$$

This expression presents similar behaviors as the ones from the kernel obtained for the interior Dirichlet Laplace problem. In particular, $K(s, t; \epsilon)$ is nearly singular when $s + t = \pi$ or $s + t = 3\pi$. When $\cos(s + t) = -1$,

$$K(s, t; \epsilon) = \frac{\sqrt{1 + \epsilon^2 - (-1 + \epsilon^2)\cos(2(\pi - s))}}{2\sqrt{2}\epsilon\sqrt{\cos^2(s) + \epsilon^2\sin^2(s)}}, \tag{3.9}$$

and so

$$\lim_{\epsilon \to 0} K(s, t; \epsilon) \to \infty. \tag{3.10}$$

Figure 3.2 shows the behavior of the kernel. We observe when $s + t = \pi$ the kernel has a nearly singular peak. As $\epsilon \to 0$, the values of the kernel at $s + t = \pi$ becomes more singular.

16
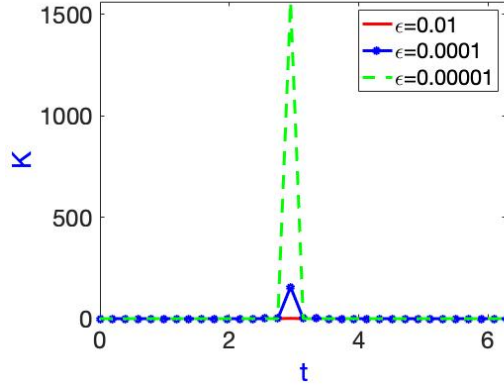
Figure 3.2: Plot showing the behavior of the kernel for a fixed $s = \frac{\pi}{16}$ with various values of ϵ.

3.2   Numerical Investigation

Like before, we use the Periodic Trapezoid Rule to discretize the BIE (3.5). The BIE when using PTR then becomes

$$\frac{1}{2}\mu(s_i) + \frac{1}{N}\sum_{j=1}^{N} K(s_i, t_j; \epsilon)\mu(t_j) = f(s_i), \quad i = 1, ...N. \tag{3.11}$$

Here $s_i = \frac{2\pi i}{N}$ and $t_j = \frac{2\pi j}{N}$, $i, j = 1, \ldots, N$. We rewrite (3.11) as the following system;

$$\left(\frac{1}{2}I_N + P_E\right)\mu_N = f_N, \tag{3.12}$$

where P_E is the matrix obtained from the discretization of the adjoint double-layer potential using PTR.

To determine the accuracy of the method we use an exact solution. Contrary to the interior Dirichlet Laplace problem, there is no explicit expression for the source f to provide an exact solution to equation (3.5). Instead we use an exact solution of (3.1) directly. We consider $u_{exact} = \frac{x - x_o}{|x - x_o|^2}$ as a solution to the exterior Neumann problem with $x_o \in D$ and use it to find $f = \frac{\partial u_{exact}}{\partial n_x}|_B$. We introduce a Cartesian grid to approximate of the single-layer potential

$$u(x) = \int_B \left(-\frac{1}{2\pi}\log|x - y|\right)\mu(y)\mathrm{d}y \tag{3.13}$$

using our approximation of μ from (3.12), we evaluate u_{exact} on the same grid and compute the error. We have tried using a body-fitted grid but obtained a large error due to the curvature of our problem (See Appendix G). A Cartesian grid works best for this problem.

3.2.1   Numerical Results

Figure 3.3a shows the approximation of μ using PTR. The peaks in the plot correspond to $t = 0$ and $t = \pi$. The anti-diagonals on the heatmap in Figure 3.3b

correspond to $s+t = \pi$ and $s+t = 3\pi$. Here, the condition number of $(\frac{1}{2}I_N + P_E)$ is 13.79133, which means that the matrix is sensitive to the inverse calculation. Recall that we care about the accuracy of the approximation and not on computational cost.

Figure 3.3c is a log plot of the absolute error. We notice that the error is larger near $x = 0$. This is consistent with the behavior of the peaks that appear in the plot of μ. From the heatmap, we observe that the kernel is nearly singular at $s+t = \pi$ and $s+t = 3\pi$. Using the same approach as in Chapter 2, we seek to provide a correction at the points where the kernel is nearly singular.

(a)

(b)

(c)
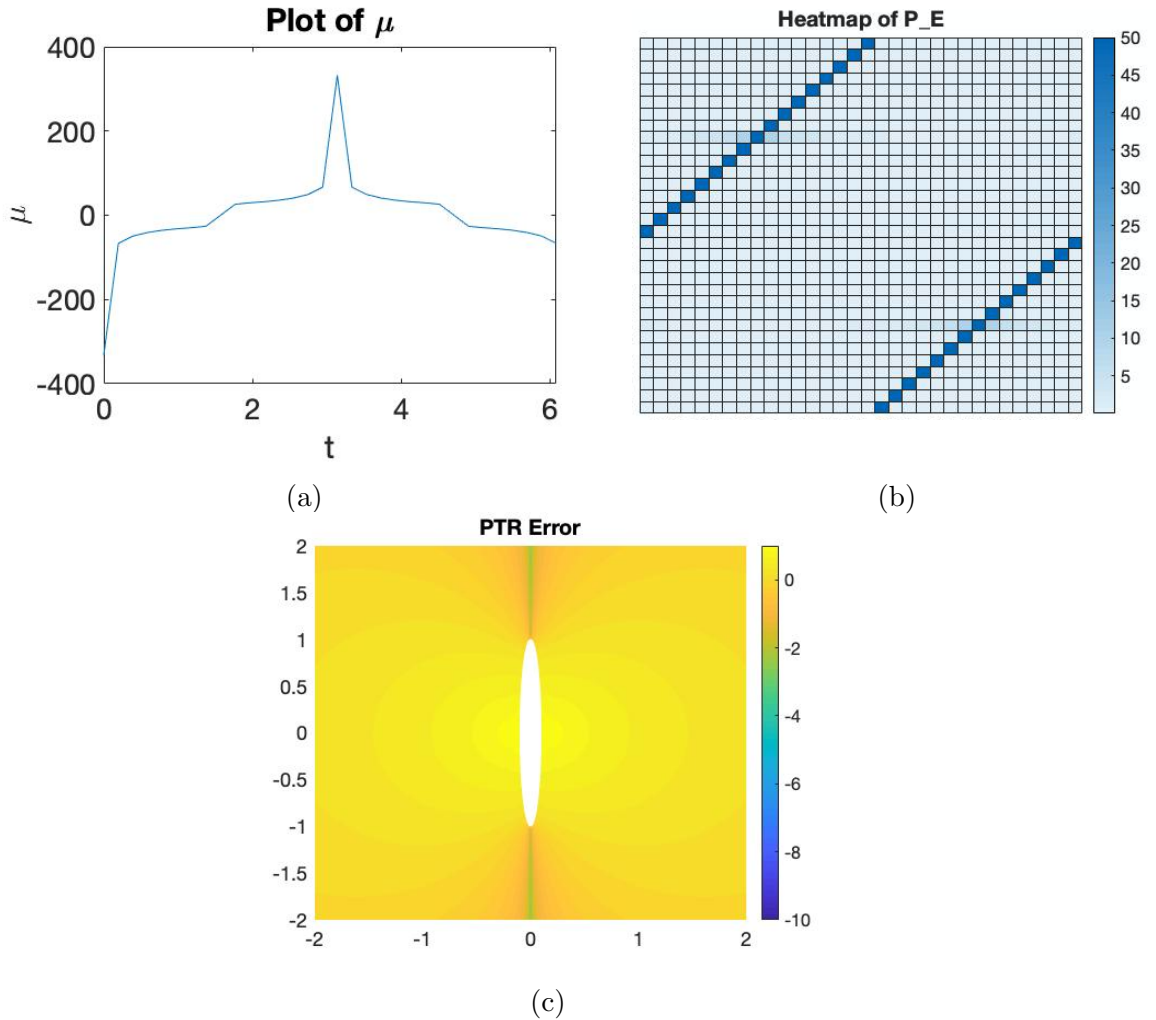
Figure 3.3: (a)Periodic Trapezoid Rule approximation of μ with $\epsilon = 0.1$ and $N = 32$. (b) Heatmap of the matrix P_E for $\epsilon = 0.01$ and $N = 32$.(c) Log plot of the absolute ($|u - u_{exact}|$) error using a $\log_{10}$ scale for PTR with $\epsilon = 0.1$ and $N = 32$.

3.3 Inner Asymptotic Expansion

We seek to improve the approximation of the Periodic Trapezoid Rule by introducing an asymptotic expansion at the points where the kernel is nearly singular:

$y(s+t) = y(\pi)$ and $y(s+t) = y(3\pi)$. We start by looking at the adjoint of the double-layer potential

$$I = \frac{1}{2\pi} \int_0^{2\pi} K(s,t;\epsilon)\mu(t)\mathrm{d}t, \tag{3.14}$$

where $K(s,t;\epsilon)$ is given in (3.7). Similar to Chapter 2 the integral is evaluated neighborhood around the point $y(t) = y(\pi - s)$. We introduce a shift so that the nearly singular behavior happens at $t = 0$ and then rescale by ϵ to obtain

$$I_1 = \frac{1}{2\pi} \int_{-\frac{\Delta t}{\epsilon}}^{\frac{\Delta t}{\epsilon}} K(s,\epsilon T + \pi - s;\epsilon)\mu(\epsilon T + \pi - s)\epsilon\mathrm{d}T. \tag{3.15}$$

Using Mathematica (see Appendix D for details) we expand the kernel K and the density μ in (3.15) about $\epsilon = 0$, take the leading order terms of the expansion, and find

$$I_1 = \frac{1}{2\pi} \int_{-\frac{\Delta t}{\epsilon}}^{\frac{\Delta t}{\epsilon}} \left(\frac{\sqrt{2}\sqrt{1+\cos(2s)}}{(4+T^2)\sqrt{\cos^2(s)}\epsilon} + \frac{\sqrt{2}T\sin(2s)}{(4+T^2)\sqrt{\cos^2(s)}\sqrt{1+\cos(2s)}} \right) \times$$
$$\mu(\pi - s)\epsilon\mathrm{d}T + O(\epsilon)$$
$$= \frac{\arctan(\frac{\Delta t}{2\epsilon})}{\pi}\mu(\pi - s) + O(\epsilon). \tag{3.16}$$

We notice that the expansion obtained is the same expansion obtained for the interior Dirichlet problem up to a sign. Therefore, the kernel for this problem has a similar behavior to the kernel of the interior Dirichlet problem. After obtaining the inner asymptotic expansion we replace PTR with the inner asymptotic expansion given in (3.16). For all other points we use the Composite Trapezoid Rule to obtain an approximation for μ. The Modified Trapezoid Rule (MTR) applied to (3.5) yields

$$\frac{1}{2}\mu(s_i) + \frac{1}{N} \sum_{\substack{j=1 \\ s_i+t_j \neq \pi \\ s_i+t_j \neq 3\pi}}^{N} K(s_i,t_j;\epsilon)\mu(t_j) + \sum_{\substack{s_i+t_j=\pi \\ s_i+t_j=3\pi}} \left(\frac{\arctan(\frac{\Delta t}{2\epsilon})}{\pi}\mu(\pi - s_i) \right) = f(s_i),$$
$$i = 1, \ldots, N. \tag{3.17}$$

We solve for μ with the system

$$\left(\frac{1}{2}I_N + M_E \right)\mu_N = f_N, \tag{3.18}$$

where M_E is the matrix of the Modified Trapezoid rule.

As above, we use $u_{exact} = \frac{x-x_o}{|x-x_o|^2}$ with $x_o \in D$ to obtain μ_N and then approximate the single-layer potential, u.

3.4 Numerical Results

Figure 3.4a is the approximation obtained using MTR. We find that μ is still peaked at $t = 0$ and $t = \pi$, but the MTR is compensating for the approximation of μ compare with the results using PTR the peaks are smaller. Figure 3.4b shows the heatmap of matrix M_E. An improvement is observed along the anti-diagonals indicated by the color scale of the heatmap. The condition number of matrix $(\frac{1}{2}I + M_E)$ is 4.378945. The correction provided a better conditioned matrix. Figure 3.4c is a plot of the absolute error which shows the error using MTR has improved slightly. We observe the same error as before near $x = 0$.

(a)

(b)

(c)
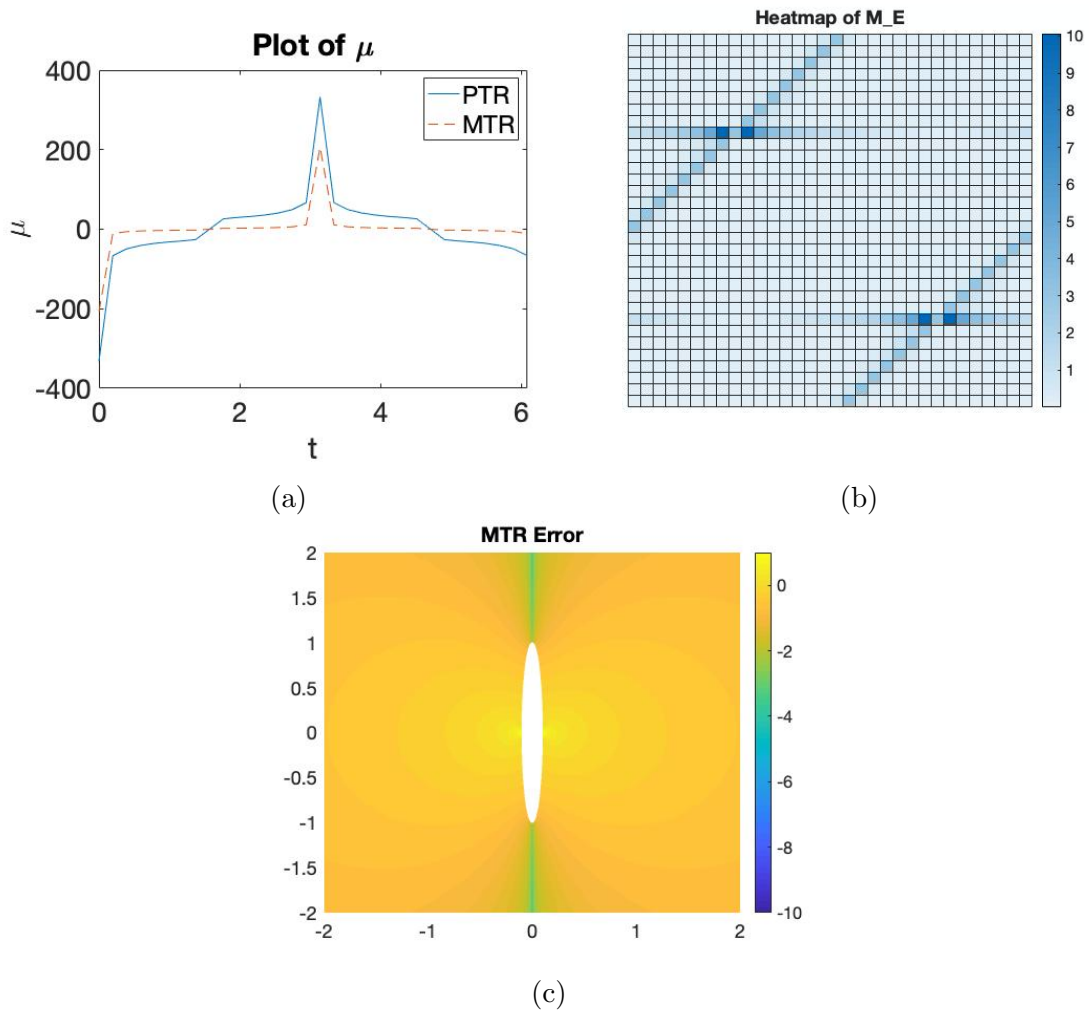
Figure 3.4: (a) Modified Trapezoid Rule approximation of μ with $\epsilon = 0.01$ and $N = 32$. (b) Heatmap of matrix M_E for MTR with $\epsilon = 0.01$ and $N = 32$. (c) Log plot of the absolute error ($|u - u_{exact}|$) using a $\log_{10}$ scale for PTR with $\epsilon = 0.1$ and $N = 32$.

3.5 Spectral method

Similarly to Chapter 2, since we have a closed curve and periodic function we are able to use a Spectral method. We consider a Fourier spectral method. We start

with the BIE

$$\frac{1}{2}\mu(s) + \frac{1}{2\pi}\int_0^{2\pi} K(s,t;\epsilon)\mu(t)\mathrm{d}t = f(s), \quad s \in [0, 2\pi]. \tag{3.19}$$

We substitute

$$\mu(s) = \sum_{n=-\infty}^{\infty} \hat{\mu}_n e^{ins} \quad \text{with} \quad \hat{\mu}_n = \frac{1}{2\pi}\int_0^{2\pi}\mu(s)e^{-ins}\mathrm{d}s \tag{3.20}$$

and we assume $f(s) = \sum_{n=-\infty}^{\infty} \hat{f}_n e^{ins}$ with $\hat{f}_n = \frac{1}{2\pi}\int_0^{2\pi} f(s)e^{-ins}\mathrm{d}s$.

Just as we have done for the interior Dirichlet problem, we substite these Fourier series representations into (3.20) and find

$$\frac{1}{2}\hat{\mu}_n + \hat{\mu}_{-n}\hat{k}_n = \hat{f}_n, \quad n = -\infty, \dots, \infty. \tag{3.21}$$

We need to find the Fourier coefficients of the Kernel $\hat{k}_n$.

Recall the kernel expression is

$$K(s,t;\epsilon) = -\frac{\epsilon\sqrt{1 + \epsilon^2 - (-1 + \epsilon^2)\cos(2t)}}{\sqrt{2}(-1 - \epsilon^2 + (-1 + \epsilon^2)\cos(s+t))\sqrt{\cos^2(s) + \epsilon^2\sin^2(s)}}. \tag{3.22}$$

The kernel is not a rational trigonometric function thus the Fourier coefficients $\hat{k}_n$ cannot be computed analytically. The expression of the kernel here is more complicated. Accurately computing these Fourier coefficients numerically will require a large number of points on the boundary. Thus, this method is not very efficient.

3.6 Comparison and Conclusion

The exterior Neuman problem for a narrow ellipse has a challenging kernel expression. Furthermore, we do not have an exact solution for the BIE. We attempted to use a body-fitted grid to obtain an approximation of u, but the grid failed to capture the regions of high curvature. A Cartesian grid was preferred due to the curvature of our problem. The heatmap of matrix P_E had large values along $s + t = \pi$ and $s + t = 3\pi$. We introduced a correction at the points where the kernel is nearly singular and the heatmap of MTR showed a slight improvement. We considered a Fourier spectral method. The Fourier coefficients $\hat{k}_n$ are not available because we do not have a kernel of a rational trigonometric form. However, the method can be implemented but requires a large number of points on the boundary which is costly. An extension worth exploring is matched asymptotics to improve the accuracy of the MTR.

Chapter 4

Extension to Scattering Problem

We study the exterior Helmholtz problem in a domain whose boundary has regions of high curvature. We seek to find $u \in C^2(E) \cup C^1(\bar{E})$ satisfying

$$
\begin{aligned}
\Delta u + k^2 u &= 0, \quad \text{in} \quad E := \mathbb{R}^2 \setminus \bar{D} \\
u &= f, \quad \text{on} \quad B \\
\lim_{|r| \to \infty} \sqrt{r} \left(\frac{\partial}{\partial r} - ik \right) u(x) &= 0, \quad \text{with} \quad r = |x|.
\end{aligned}
\tag{4.1}
$$

The last equation in (4.1) is the Sommerfeld radiation condition [8, 4]. Above, f denotes the source, and k is the wavenumber associated with the source. We seek to solve (4.1) outside an ellipse as represented in Figure 4.1
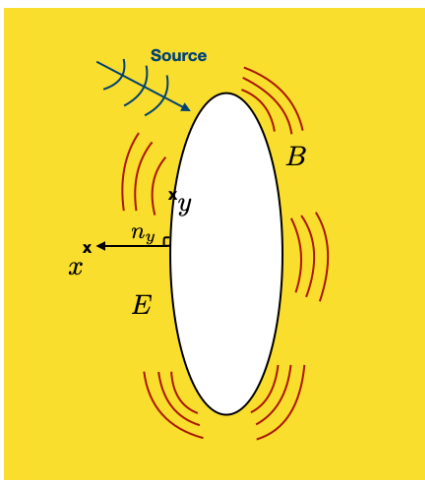
Figure 4.1: Notations and sketch for the scattering problem.

The solution of problem (4.1) can be represented as a combination of the double- and single-layer potential [17],

$$
u(x) = \int_B \left(\frac{\partial G}{\partial n_y}(x, y) - ik G(x, y) \right) \mu(y) \mathrm{d}\sigma_y, \quad x \in E,
\tag{4.2}
$$

where $G(x, y)$ is the Green's function to Helmholtz equation in 2D is given by

$$G(x, y) = \frac{i}{4} H_0^{(1)}(k|x - y|). \tag{4.3}$$

where $H_0^{(1)}(\cdot)$ denotes the Hankel function of the first kind. The density μ, satisfies the following BIE

$$\frac{1}{2}\mu(x) + \int_B \left(\frac{\partial G}{\partial n_y}(x, y) - ikG(x, y) \right) \mu(y)\mathrm{d}\sigma_y = f(x), \quad x \in B. \tag{4.4}$$

4.1 Parameterization

We make use of explicit parameterization $y = y(t) = \langle y_1(t), y_2(t) \rangle$ where $0 \le t \le 2\pi$ and for $x \in B$, we write $x = y(s)$ for $s \in [0, 2\pi]$, $\mu(y(t)) = \mu(t)$ and $f(x) = f(s)$. The BIE then becomes

$$\frac{1}{2}\mu(s) - \int_0^{2\pi} \left(\frac{ik}{4} H_1^{(1)}(k|y(s) - y(t)|)n(t) \cdot \frac{y(s) - y(t)}{|y(s) - y(t)|} \right.$$
$$\left. + \frac{k}{4} H_0^{(1)}(k|y(s) - y(t)|) \right) |y'(t)|\mu(t)\mathrm{d}t = f(s) \tag{4.5}$$

where $\quad 0 \le s \le 2\pi$, $n_y = n(y(t))$ and $|y'(t)|$ denoting the Jacobian.

After plugging in the parameterization for the ellipse, we rewrite (4.5) as

$$\frac{1}{2}\mu(s) - \int_0^{2\pi} [L(s, t; \epsilon) + ikM(s, t; \epsilon)]\,\mu(t)\mathrm{d}t = f(s) \tag{4.6}$$

with

$$L(s, t; \epsilon) = \frac{ik}{4} H_1^{(1)}(kr(s, t; \epsilon)) \frac{\epsilon \cos(t)(\cos(s) - \cos(t)) + \epsilon \sin(t)(\sin(s) - \sin(t))}{\epsilon(\cos(s) - \cos(t)))^2 + (\sin(s) - \sin(t))^2}$$
$$= \frac{ik}{4} H_1^{(1)}(kr(s, t; \epsilon)) \frac{\epsilon}{-1 - \epsilon^2 + (-1 + \epsilon^2)\cos(s + t)}, \tag{4.7}$$

$$M(s, t; \epsilon) = \frac{i}{4} H_0^{(1)}(kr(s, t; \epsilon))\sqrt{\epsilon^2 \sin^2(t) + \cos^2(t)}, \tag{4.8}$$

where $r(s, t; \epsilon) = \sqrt{\epsilon^2(\cos(s) - \cos(t))^2 + (\sin(s) - \sin(t))^2}$.

Contrary to the Laplace problems we have a singular kernel when $s = t$, we get a log singularity because of the Hankel functions. Because we have a log singularity, we are not able to use the Periodic Trapezoid Rule to approximate the BIE. We use an alternative quadrature method that is able to treat the log singularity of the kernel, called Kress quadrature [17].

In equation (4.7) we notice that the rational expression is the same expression as the kernel for the interior Dirichlet Laplace problem. Just like the interior Dirichlet Laplace problem we have a nearly singular behavior when $s + t = \pi$ and $s + t = 3\pi$. When $\cos(s + t) = -1$ we obtain

$$L(s, t; \epsilon) = -\frac{ik}{4} H_1^{(1)}(kr(s, t; \epsilon)) \frac{1}{2\epsilon}, \tag{4.9}$$

which leads to

$$\lim_{\epsilon \to 0} L(s, t; \epsilon) = -\infty. \tag{4.10}$$

Figure 4.2 shows the behavior of the kernel with different values of ϵ. We observe that there is a sharp peak occurring at $s + t = \pi$ and $s + t = 3\pi$ which means the kernel is nearly singular at those points. We observe a singularity occurring at $s = t$ and as $\epsilon \to 0$, the peak at $s + t = \pi$ and $s + t = 3\pi$ gets sharper. The kernel is challenging because we have to work with both a singular and nearly singular behaviors.
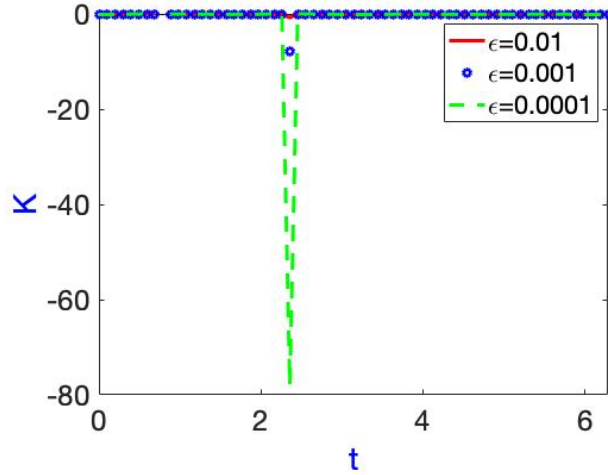
Figure 4.2: Plot showing the behavior of the kernel for $s = \frac{\pi}{64}$ and $\epsilon = 10^{-2}, 10^{-3}$, and 10^{-4}.

4.2 Kress quadrature

We use Kress quadrature [17] to discretize the BIE (4.6)

$$\frac{1}{2}\mu(s) - \int_0^{2\pi} [L(s, t; \epsilon) + ikM(s, t; \epsilon)] \, \mu(t) \mathrm{d}t = f(s). \tag{4.11}$$

Kress quadrature treats logarithmic singularities by breaking up the kernel, $L(s, t; \epsilon) + ikM(s, t; \epsilon)$ as follows:

$$L(s, t; \epsilon) = L_1(s, t; \epsilon) \ln\left(4\sin^2\left(\frac{s-t}{2}\right)\right) + L_2(s, t; \epsilon) \tag{4.12}$$

and $\tag{4.13}$

$$M(s, t; \epsilon) = M_1(s, t; \epsilon) \ln\left(4\sin^2\left(\frac{s-t}{2}\right)\right) + M_2(s, t\epsilon) \tag{4.14}$$

where $\ln\left(4\sin^2\left(\frac{s-t}{2}\right)\right)$ is used to treat the singularity.

24

Here we define L_1, L_2, M_1 and M_2 as;

for $s \neq t$

$$L_1(s, t; \epsilon) := \frac{k}{2\pi}(\cos(t)(\epsilon\cos(s) - \epsilon\cos(t)) + \epsilon\sin(t)(\sin(s) - \sin(t)))\frac{J_1(k, r(s, t; \epsilon))}{r(s, t; \epsilon)}$$

$$(4.15)$$

$$L_2(s, t; \epsilon) := L(s, t; \epsilon) - L_1(s, t; \epsilon)\ln\left(4\sin^2\left(\frac{s - t}{2}\right)\right) \tag{4.16}$$

$$M_1(s, t; \epsilon) := -\frac{1}{2\pi}J_0(kr(s, t; \epsilon))\sqrt{\epsilon^2\sin^2(t) + \cos^2(t)} \tag{4.17}$$

$$M_2(s, t; \epsilon) := M(s, t; \epsilon) - M_1(s, t; \epsilon)\ln\left(4\sin^2\left(\frac{s - t}{2}\right)\right) \tag{4.18}$$

for $s = t$

$$L_2(s, s; \epsilon) := \frac{1}{2\pi}\frac{-\epsilon\sin^2(s) + \epsilon\cos^2(s)}{\epsilon^2\sin^2(s) + \cos^2(s)} \tag{4.19}$$

$$M_2(s, s; \epsilon) := \left[\frac{i}{2} - \frac{C}{\pi} - \frac{1}{2\pi}\ln(\frac{k^2}{4}(\epsilon^2\cos^2(s) + \sin^2(s)))\right]\sqrt{\epsilon^2\sin^2(s) + \cos^2(s)} \tag{4.20}$$

where C is Euler's constant. Combining the terms, we define

$K_1(s, t; \epsilon) = L_1(s, t; \epsilon) + ikM_1(s, t; \epsilon)$, $K_2(s, t; \epsilon) = L_2(s, t; \epsilon) + ikM_2(s, t; \epsilon)$, and we discretize the BIE (4.11) as,

$$\mu_i^{(n)} - \sum_{k=0}^{2n-1}[R_{|i-k|}^{(n)}K_1(s_i, t_k) + \frac{\pi}{n}K_2(s_i, t_k)]\mu_k^{(n)} = 2f(s_i), \quad i = 0, \cdots, 2n-1, \tag{4.21}$$

with the quadrature weights

$$R_k^{(n)} := -\frac{2\pi}{n}\sum_{m=1}^{n-1}\frac{1}{m}\cos\left(\frac{mk\pi}{n} - \frac{(-1)^k\pi}{n^2}\right), \quad k = 0, \cdots, 2n - 1. \tag{4.22}$$

This results in the following system

$$(I_N - H)\mu_N = 2f_N, \tag{4.23}$$

where H is the matrix obtained from the Kress quadrature discretization.

In order to estimate the accuracy of the method we use an exact solution. Similar to the exterior Neumann Laplace problem, there is no explicit expression for the source, f, to provide an exact solution to equation (4.5). Here we use an exact solution of (4.1) directly. We consider $u_{exact} = \frac{i}{4}H_0^{(1)}(k|x - x_0|)$ as a solution to the exterior Helmholtz problem with $x_o \in D$ and use it to find $f = u_{exact}|_B$. We use a Cartesian grid to approximate u_{exact} and obtain an approximation of the single- and double-layer potential

$$u(x) = \int_B \left(\frac{\partial G}{\partial n_y}(x, y) - ikG(x, y)\right)\mu(y)\mathrm{d}y. \tag{4.24}$$

We have tried using a body-fitted but obtained a large error due to the curvature of our problem (See Appendix H). Similar to the exterior Neumann problem we found that a Cartesian grid works best for this problem since it captures the curvature of our problem.

4.3   Numerical Results

Figure 4.3a represents the approximation of μ using Kress quadrature. The peaks in the plot correspond to $t = 0, \pi$. Figure 4.3b represents the heatmap of the absolute value of matrix H. We observe big values along the anti-diagonals which correspond to where the kernel is nearly singular ($s + t = \pi$ and $s + t = 3\pi$). The condition number of matrix ($I_N - H$) is 2.931205. We notice that the condition number is bigger than 1 which means the matrix is sensitive to inverse calculation. In Figure 4.3c is a log plot of the error ($|u - u_{exact}|$). We notice that the error is bigger near $x = 0$ which is consistent to the behavior observed in the plot of μ. In Figure 4.3d we observe as $\epsilon \to 1$ the error increases and as $\epsilon \to 0$ the error decreases. For small values of ϵ we get an accuracy of $O(1)$. Next we seek to improve the approximation by making a correction at the points where the kernel is nearly singular.

Figure 4.3: (a) Approximation of μ with $\epsilon = 0.001$, $N = 120$ and $k = 5$. (b) Heatmap of the absolute value of matrix H with $\epsilon = 0.001$, $N = 64$ and $k = 5$. (c) Log plot of the absolute error ($|u - u_{exact}|$) using a $\log_{10}$ scale for Kress quadrature with $\epsilon = 0.01$ and $N = 120$. (d) Log-log plot of error ($||u - u_{exact}||_\infty$) vs. ϵ with $N = 128$.

4.4 Inner Asymptotic expansion

We seek to make a correction to Kress quadrature by introducing an asymptotic expansion at the points where the kernel is nearly singular $y(s + t) = y(\pi)$ and $y(s + t) = y(3\pi)$. We start by looking at the single- and double-layer potential

$$I = \int_0^{2\pi} (L(s, t; \epsilon) + ikM(s, t; \epsilon))\mu(t)\mathrm{d}t \tag{4.25}$$

Similar to Chapter 2 the integral is evaluated at a neighborhood around the point $y(t) = y(\pi - s)$. After a series of substitutions, we introduce a shift so that the nearly singular behavior happens at $t = 0$ and then rescale by ϵ to obtain

$$I_1 = \frac{1}{2\pi} \int_{-\frac{\Delta t}{\epsilon}}^{\frac{\Delta t}{\epsilon}} (L(s, \epsilon T + \pi - s; \epsilon) + ikM(s, \epsilon T + \pi - s; \epsilon))\mu(\epsilon T + \pi - s)\epsilon\mathrm{d}T. \tag{4.26}$$

Using Mathematica (see Appendix E for details) we expand the kernel and density in (4.26) about $\epsilon = 0$. We provide asymptotic expansions only for L since it is the only part of the kernel that exhibits a near singular behavior, we obtain

$$\int_{-\frac{\Delta t}{\epsilon}}^{\frac{\Delta t}{\epsilon}} L_1(s, \epsilon T + \pi - s; \epsilon)\mu(\epsilon T + \pi - s)\mathrm{d}T = \frac{k^2 \Delta t \epsilon \cos^2(s)\mu(\pi - s)}{2\pi} + O(\epsilon),$$

(4.27)

and

$$\int_{-\frac{\Delta t}{\epsilon}}^{\frac{\Delta t}{\epsilon}} L_2(s, \epsilon T + \pi - s; \epsilon)\mu(\epsilon T + \pi - s)\mathrm{d}T = \frac{2\arctan(\frac{\Delta t}{2\epsilon})\mu(\pi - s)}{\pi} + O(\epsilon).$$

(4.28)

We notice that the expansion obtained for L_2 is similar to the expansion of the interior Dirichlet problem. We plug in Kress quadrature with the expansion obtained in (4.27) and (4.28), and for all other points we used Kress quadrature. We rewrite (4.21) and add the asymptotic terms for $s + t = \pi$ and $s + t = 3\pi$. We solve the following system for μ,

$$(I_N - M_H)\mu_N = 2f_N,$$

(4.29)

where M_H is the matrix obtained by the discretization of the Modified Kress method. We use μ_N to obtain an approximation for u, the single- and double-layer potential.

4.5   Numerical Results

Figure 4.4a is a plot of μ with different values of ϵ. We see that μ is still peaked at $t = 0, \pi$. Figure 4.4b is the heatmap of the absolute values of matrix M_H. The color scale of the heatmap is significantly smaller. The condition number of matrix $(I_N - M_H)$ is 1.123853, compared to the condition number obtained from the system using Kress quadrature matrix, $(I_N - M_H)$, this matrix is much better conditioned. Figure 4.5a is a plot of the log of the error $(|u - u_{exact}|)$. We observe a small correction, and the same error as before near $x = 0$. In Figure 4.5b we observe that as $\epsilon \to 0$ the approximation of the Modified Kress method offers more accuracy than Kress quadrature. Overall, we observed that the Modified Kress method makes correction at the points where the kernel is nearly singular.
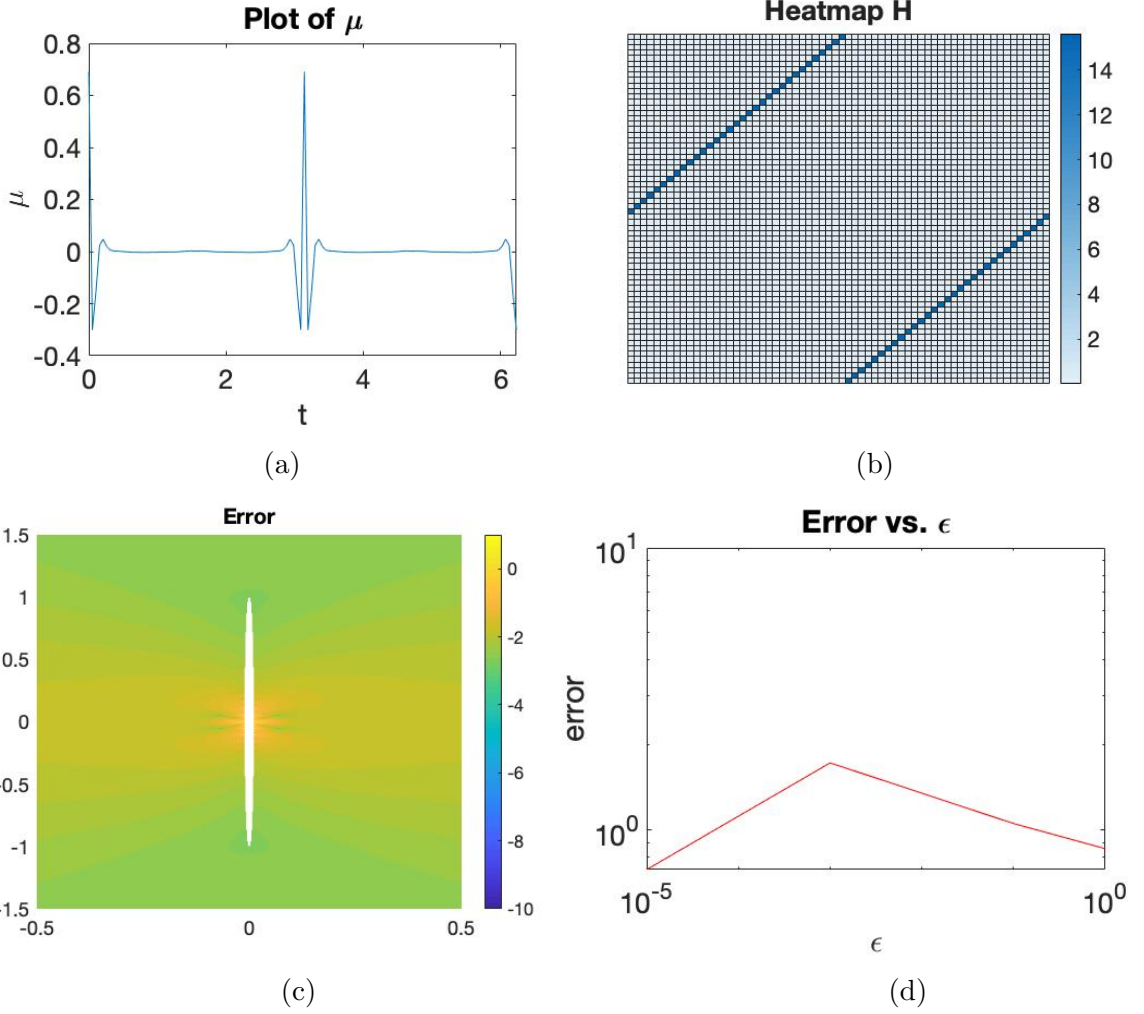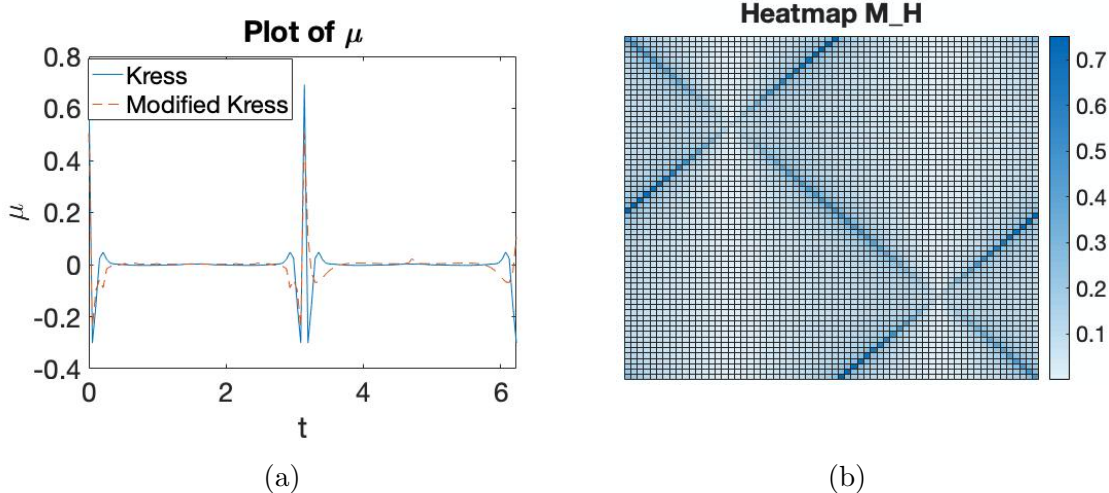
Figure 4.4: (a) Approximation of μ with $\epsilon = 0.001$, $N = 120$ and $k = 5$. (b) Heatmap of the absolute value of matrix H with $\epsilon = 0.001$, $N = 64$ and $k = 5$.
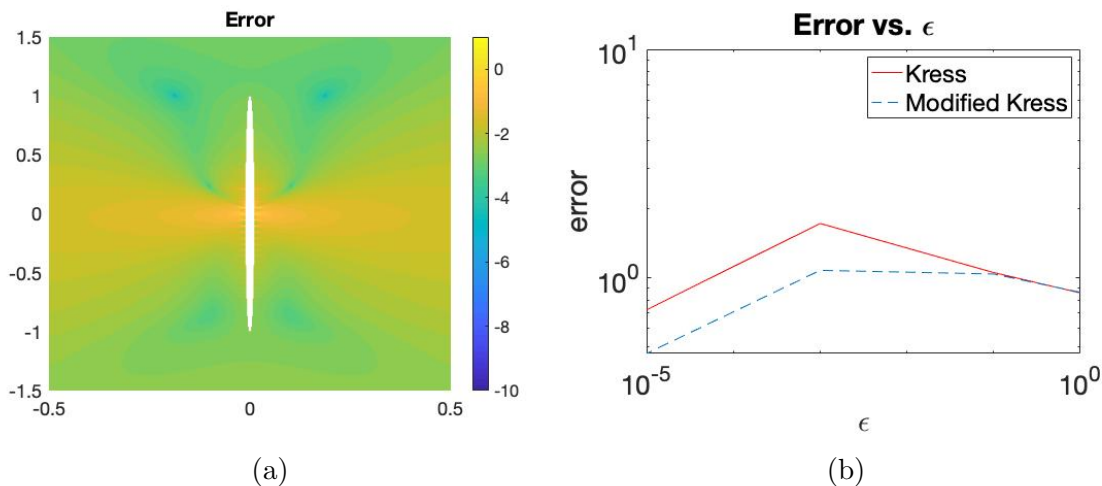
Figure 4.5: (a) Log plot of the absolute error ($|u - u_{exact}|$) using a $\log_{10}$ scale for Kress quadrature with $\epsilon = 0.01$ and $N = 120$. (b) Log-log plot of error ($||u - u_{exact}||_\infty$) vs. ϵ with $N = 128$.

4.6 Conclusion

The exterior Helmholtz problem for regions of high curvature is challenging due to a singular kernel in the BIE and the nearly singular behaviors that appear. Because the kernel is singular, PTR does not work, and we use Kress quadrature to obtain an approximation. We offer a correction to Kress quadrature using an inner asymptotic expansion and the results show improvement. Future work includes using a spectral method and matched asymptotics for this problem.

Chapter 5

Summary

We have investigated the behavior of layer potentials in regions of high curvature and made modifications to two quadrature methods (PTR and Kress quadrature) using an inner asymptotic expansion. Regions of high curvature produce nearly singular behavior of the kernel which produces a large error when approximating a layer potential. Using the information where the kernel is nearly singular, we made a correction to improve the existing method. The numerical results of the modified method showed improvements on the existing methods. A spectral approximation was obtained but was limited to a rational trigonometric kernel. A spectral approximation could still be obtained for kernels that did not have a rational trigonometric form however required a large number of points on the boundary which is costly. Future work would include doing an extension of the problems presented in Chapters 3 and 4 and conducting matched asymptotics to improve the modified methods. Another extension of the modified method would be to implement the method for other boundaries with regions of high curvature i.e. a cylindrical rod or an elliptical star.

Appendix A

Proof of Representation formula

In this section we establish the representation formula which represents the solution of Laplace's equation in $2D$ via layer potentials. To proof the representation formula, we will use the solution to the Laplace equation and Green's second identity. Consider D to be a $2D$ domain, B is the boundary and $u \in C^2(D) \cap C^1(\bar{D})$ is harmonic solution in D. It satisfies $\Delta u = 0$. The fundamental solution of the Laplace equation is given by

$$w(r) = -\frac{1}{2\pi} \log(r) = -\frac{1}{2\pi} \log(|x - y|), \quad x, y \in D. \tag{A.1}$$
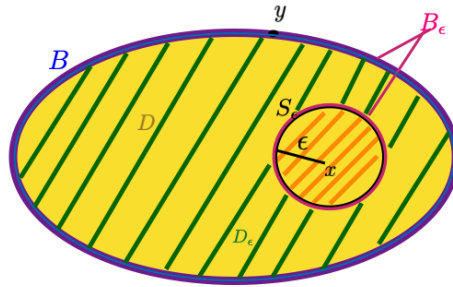
If we apply u and $v = -\frac{1}{2\pi} \log(r)$ to Green's second identity where $x \in D$ is fixed and the take the integration with respect to $y \in B$ then the identity has a singularity of v at $x = y$. So we exclude a small disk from D, denoted as $K_\epsilon(x)$ centered at x and radius $\epsilon > 0$ so that $K_\epsilon(x) \subset D$. Figure 1 illustrates the domain and boundary which we are working in:

D : domain which is represented in yellow

B : boundary represented in blue

S_ϵ : circle which is the boundary of the disk $K_\epsilon(x)$ represented in black

B_ϵ : $B \cup S_\epsilon$ the union of the 2 boundaries in pink.

D_ϵ : Is D minus the disk $K_\epsilon(x)$ represented in green.

$K_\epsilon(x)$: disk of radius ϵ and center x represented in orange

Now we apply u and $v = -\frac{1}{2\pi} \log(r)$ to Green's second identity on the domain

$D_\epsilon = D \setminus K_\epsilon(x)$ with boundary $B_\epsilon = B \cup S_\epsilon(x)$ to get

$$\int_{D_\epsilon} \left[\left(-\frac{1}{2\pi} \log(r) \right) \Delta u - u\Delta\left(-\frac{1}{2\pi} \log(r) \right) \right] dy =$$
$$\int_{B_\epsilon} \left[\left(-\frac{1}{2\pi} \log(r) \right) \frac{\partial u}{\partial n} - u\frac{\partial}{\partial n}\left(-\frac{1}{2\pi} \log(r) \right) \right] d\sigma_y \qquad \text{(A.2)}$$

$$= \int_B \left[\left(-\frac{1}{2\pi} \log(r) \right) \frac{\partial u}{\partial n} - u\frac{\partial}{\partial n}\left(-\frac{1}{2\pi} \log(r) \right) \right] d\sigma + \int_{S_\epsilon} \left(-\frac{1}{2\pi} \log(r) \right) \frac{\partial u}{\partial n} d\sigma \quad \text{(A.3)}$$

Now looking at the left hand side integral of (A.2)

$$\lim_{\epsilon \to 0}\left[\int_{D_\epsilon} \left(-\frac{1}{2\pi} \log(r) \right) \Delta u dy \right] \to \int_D \left(-\frac{1}{2\pi} \log(r) \right) \Delta u dy \qquad \text{(A.4)}$$

Since u has continuous partial derivatives in D we can assume $\frac{\partial u}{\partial n} = |\nabla u \cdot n| \leq M$ for some constant M and all points in $y \in B$ are in a fixed neighborhood of x then

$$\left| \int_{S_\epsilon} \left(-\frac{1}{2\pi} \log(r) \right) \frac{\partial u}{\partial n} d\sigma_y \right| \leq \frac{M}{2\pi} \log(\epsilon) \int_{S_\epsilon} d\sigma_y = \frac{M}{2\pi} \log(\epsilon)(2\pi\epsilon) \to 0 \ \ as \ \epsilon \to 0.$$
$$\text{(A.5)}$$

Now we consider part of the integral of equation over the disk of equation (A.3)

$$\int_{S_\epsilon} u\frac{\partial}{\partial n}\left(-\frac{1}{2\pi} \log(r) \right) d\sigma_y \qquad \text{(A.6)}$$

The outward unit normal to S_ϵ is $n_y = \frac{x-y}{r}$ and

$$-\frac{1}{2\pi} \frac{\partial}{\partial n_y}(\log(r)) = -\frac{1}{2\pi} \nabla_y(\log(r)) \cdot n_y = -\frac{1}{2\pi} \frac{x-y}{r} \cdot \left(-\frac{x-y}{r^2} \right) = \frac{1}{2\pi r} \quad \text{(A.7)}$$

Using polar coordinates centered at x we obtain

$$\int_{S_\epsilon} u\frac{\partial}{\partial n}\left(\frac{1}{2\pi} \log(r) \right) d\sigma = \int_0^{2\pi} \frac{1}{2\pi\epsilon} u(x + \epsilon\omega)\epsilon d\theta \qquad \text{(A.8)}$$

where $\omega = (r, \theta)$. Taking the limit as $\epsilon \to 0$ we get

$$\lim_{\epsilon \to 0} \left[\int_{S_\epsilon} u\frac{\partial}{\partial n}\left(-\frac{1}{2\pi} \log(r) \right) d\sigma_y \right] = \frac{1}{2\pi} \int_0^{2\pi} u(x)d\theta = u(x) \qquad \text{(A.9)}$$

Taking equation (A.3) as $\epsilon \to 0$ we get the following result

$$u(x) = \int_B \left(-\frac{1}{2\pi} \log(r) \right) \frac{\partial u}{\partial n} d\sigma_y - \int_B u\frac{\partial}{\partial n}\left(-\frac{1}{2\pi} \log(r) \right) d\sigma_y - \int_D \left(-\frac{1}{2\pi} \log(r) \right) \Delta u dy$$
$$\text{(A.10)}$$

The solution is composed of the single-layer potential which is the first integral over B and a double-layer potential which is the second integral over B. The volume potential which is the integral over D vanishes if we let u satisfy Laplace equation such that $\Delta u = 0$ so that we get

$$u(x) = \int_B \left(-\frac{1}{2\pi} \log(r) \right) \frac{\partial u}{\partial n} d\sigma_y - \int_B u\frac{\partial}{\partial n}\left(-\frac{1}{2\pi} \log(r) \right) d\sigma_y. \qquad \text{(A.11)}$$

which is the representation formula.

Appendix B

Interior Dirichlet Inner Asymptotic Expansion

We expand the kernel to order ϵ, about ϵ=0 and then integrate:

$\text{Series}\left[\dfrac{\epsilon}{-1-\epsilon^2-\left(1-\epsilon^2\right)\text{Cos}[\pi+\epsilon*\text{T}]},\{\epsilon,0,5\}\right]$

$\dfrac{1}{\left(-2-\frac{\text{T}^2}{2}\right)\epsilon}+\dfrac{\left(-12\,\text{T}^2-\text{T}^4\right)\epsilon}{6\left(4+\text{T}^2\right)^2}+\dfrac{\left(-480\,\text{T}^4-52\,\text{T}^6-3\,\text{T}^8\right)\epsilon^3}{360\left(4+\text{T}^2\right)^3}+$

$\dfrac{\left(-11\,424\,\text{T}^6-864\,\text{T}^8-82\,\text{T}^{10}-5\,\text{T}^{12}\right)\epsilon^5}{15\,120\left(4+\text{T}^2\right)^4}+O[\epsilon]^6$

$\dfrac{1}{2*\pi}*\text{Integrate}\left[\left(\dfrac{1}{\left(-2-\frac{\text{T}^2}{2}\right)\epsilon}\right)*(\mu[\pi-\text{s}])*\epsilon,\left\{\text{T},-\dfrac{\delta}{\epsilon},\dfrac{\delta}{\epsilon}\right\}\right]$

$\text{ConditionalExpression}\left[-\dfrac{\text{ArcTan}\left[\frac{\delta}{2\,\epsilon}\right]\mu[\pi-\text{s}]}{\pi},\text{Re}\left[\frac{\epsilon}{\delta}\right]\neq0\,||\,\text{Im}\left[\frac{\epsilon}{\delta}\right]>\dfrac{1}{2}\,||\,\text{Im}\left[\frac{\epsilon}{\delta}\right]<-\dfrac{1}{2}\right]$

Appendix C

Checking that u satisfies Laplace equation

Checking that $u = \dfrac{x - x_0}{|x - x_0|^2}$ is a solution to the Laplace equation

Since we know we are solving a 2D problem then the elements of u are

$$u = \left\{ \frac{x_1 - y_1}{(x_1 - y_1)^2 + (x_2 - y_2)^2}, \frac{x_2 - y_2}{(x_1 - y_1)^2 + (x_2 - y_2)^2} \right\}$$

We first check if the first element $u = \dfrac{x_1 - y_1}{(x_1 - y_1)^2 + (x_2 - y_2)^2}$ satisfies the Laplace equation

*Obtaining the second derivative u_{x_1}

$$\text{D}\left[\frac{x_1 - y_1}{(x_1 - y_1)^2 + (x_2 - y_2)^2}, x_1 \right]$$

$$-\frac{2(x_1 - y_1)^2}{\left((x_1 - y_1)^2 + (x_2 - y_2)^2\right)^2} + \frac{1}{(x_1 - y_1)^2 + (x_2 - y_2)^2}$$

$$\text{Simplify}\left[-\frac{2(x_1 - y_1)^2}{\left((x_1 - y_1)^2 + (x_2 - y_2)^2\right)^2} + \frac{1}{(x_1 - y_1)^2 + (x_2 - y_2)^2} \right]$$

$$\frac{-(x_1 - y_1)^2 + (x_2 - y_2)^2}{\left((x_1 - y_1)^2 + (x_2 - y_2)^2\right)^2}$$

*Obtaining the second partial derivative u_{x_2}

$$D\left[\frac{x_1 - y_1}{(x_1 - y_1)^2 + (x_2 - y_2)^2}, x_2\right]$$

$$-\frac{2 (x_1 - y_1) (x_2 - y_2)}{\left((x_1 - y_1)^2 + (x_2 - y_2)^2\right)^2}$$

*Obtaining the second derivative $u_{x_1 x_1}$

$$D\left[\frac{-(x_1 - y_1)^2 + (x_2 - y_2)^2}{\left((x_1 - y_1)^2 + (x_2 - y_2)^2\right)^2}, x_1\right]$$

$$-\frac{4 (x_1 - y_1) \left(-(x_1 - y_1)^2 + (x_2 - y_2)^2\right)}{\left((x_1 - y_1)^2 + (x_2 - y_2)^2\right)^3} - \frac{2 (x_1 - y_1)}{\left((x_1 - y_1)^2 + (x_2 - y_2)^2\right)^2}$$

`Simplify[%16]`

$$\frac{2 (x_1 - y_1) \left(x_1^2 - 3 x_2^2 - 2 x_1 y_1 + y_1^2 + 6 x_2 y_2 - 3 y_2^2\right)}{\left(x_1^2 + x_2^2 - 2 x_1 y_1 + y_1^2 - 2 x_2 y_2 + y_2^2\right)^3}$$

*Obtaining the second partial derivative $u_{x_2 x_2}$

$$D\left[-\frac{2 (x_1 - y_1) (x_2 - y_2)}{\left((x_1 - y_1)^2 + (x_2 - y_2)^2\right)^2}, x_2\right]$$

$$-\frac{2 (x_1 - y_1)}{\left((x_1 - y_1)^2 + (x_2 - y_2)^2\right)^2} + \frac{8 (x_1 - y_1) (x_2 - y_2)^2}{\left((x_1 - y_1)^2 + (x_2 - y_2)^2\right)^3}$$

`Simplify[%18]`

$$\frac{2 (x_1 - y_1) \left(-(x_1 - y_1)^2 + 3 (x_2 - y_2)^2\right)}{\left((x_1 - y_1)^2 + (x_2 - y_2)^2\right)^3}$$

**Checking that $u_{x_1 x_1} + u_{x_2 x_2} = 0$

$$\frac{2 (x_1 - y_1) \left(x_1^2 - 3 x_2^2 - 2 x_1 y_1 + y_1^2 + 6 x_2 y_2 - 3 y_2^2\right)}{\left(x_1^2 + x_2^2 - 2 x_1 y_1 + y_1^2 - 2 x_2 y_2 + y_2^2\right)^3} + \frac{2 (x_1 - y_1) \left(-(x_1 - y_1)^2 + 3 (x_2 - y_2)^2\right)}{\left((x_1 - y_1)^2 + (x_2 - y_2)^2\right)^3}$$

$$\frac{2 (x_1 - y_1) \left(-(x_1 - y_1)^2 + 3 (x_2 - y_2)^2\right)}{\left((x_1 - y_1)^2 + (x_2 - y_2)^2\right)^3} + \frac{2 (x_1 - y_1) \left(x_1^2 - 3 x_2^2 - 2 x_1 y_1 + y_1^2 + 6 x_2 y_2 - 3 y_2^2\right)}{\left(x_1^2 + x_2^2 - 2 x_1 y_1 + y_1^2 - 2 x_2 y_2 + y_2^2\right)^3}$$

`Simplify[%20]`

0

Thus we conclude that $u_{x_1 x_1} + u_{x_2 x_2} = 0$

Now we check that $u = \frac{x_2 - y_2}{(x_1 - y_1)^2 + (x_2 - y_2)^2}$ satisfies the Laplace

equation

*Obtaining the second derivative u_{x_1}

$$D\left[\frac{x_2 - y_2}{(x_1 - y_1)^2 + (x_2 - y_2)^2}, x_1\right]$$

$$-\frac{2 (x_1 - y_1) (x_2 - y_2)}{\left((x_1 - y_1)^2 + (x_2 - y_2)^2\right)^2}$$

*Obtaining the second derivative $u_{x_1 x_1}$

$$D\left[-\frac{2 (x_1 - y_1) (x_2 - y_2)}{\left((x_1 - y_1)^2 + (x_2 - y_2)^2\right)^2}, x_2\right]$$

$$-\frac{2 (x_1 - y_1)}{\left((x_1 - y_1)^2 + (x_2 - y_2)^2\right)^2} + \frac{8 (x_1 - y_1) (x_2 - y_2)^2}{\left((x_1 - y_1)^2 + (x_2 - y_2)^2\right)^3}$$

Simplify[%305]

$$\frac{2 (x_1 - y_1) \left(-(x_1 - y_1)^2 + 3 (x_2 - y_2)^2\right)}{\left((x_1 - y_1)^2 + (x_2 - y_2)^2\right)^3}$$

*Obtaining the second partial derivative u_{x_2}

$$D\left[\frac{x_2 - y_2}{(x_1 - y_1)^2 + (x_2 - y_2)^2}, x_2\right]$$

$$\frac{1}{(x_1 - y_1)^2 + (x_2 - y_2)^2} - \frac{2 (x_2 - y_2)^2}{\left((x_1 - y_1)^2 + (x_2 - y_2)^2\right)^2}$$

Simplify$\left[\frac{1}{(x_1 - y_1)^2 + (x_2 - y_2)^2} - \frac{2 (x_2 - y_2)^2}{\left((x_1 - y_1)^2 + (x_2 - y_2)^2\right)^2}\right]$

$$\frac{(x_1 - y_1)^2 - (x_2 - y_2)^2}{\left((x_1 - y_1)^2 + (x_2 - y_2)^2\right)^2}$$

*Obtaining the second derivative $u_{x_2 x_2}$

$$D\left[\frac{(x_1 - y_1)^2 - (x_2 - y_2)^2}{\left((x_1 - y_1)^2 + (x_2 - y_2)^2\right)^2}, x_2\right]$$

$$-\frac{4 \left((x_1 - y_1)^2 - (x_2 - y_2)^2\right) (x_2 - y_2)}{\left((x_1 - y_1)^2 + (x_2 - y_2)^2\right)^3} - \frac{2 (x_2 - y_2)}{\left((x_1 - y_1)^2 + (x_2 - y_2)^2\right)^2}$$

Simplify[%311]

$$\frac{2 (x_2 - y_2) \left(-3 x_1^2 + x_2^2 + 6 x_1 y_1 - 3 y_1^2 - 2 x_2 y_2 + y_2^2\right)}{\left(x_1^2 + x_2^2 - 2 x_1 y_1 + y_1^2 - 2 x_2 y_2 + y_2^2\right)^3}$$

**Checking that $u_{y_1 y_1} + u_{y_2 y_2} = 0$

Appendix D

Exterior Neumann Inner Asymptotic Expansion

■ **Exterior Neumann - Asymptotic expansion/ calculation**

```
---------------------- Kernel simplification
---------------------------------
```

$$\left(\left(\left(\epsilon*\text{Cos}[s]*(\text{Cos}[s]-\text{Cos}[t])\right)+\left(\epsilon*\text{Sin}[s]*(\text{Sin}[s]-\text{Sin}[t])\right)\right)*\right.$$
$$\left.\left(\epsilon^2*(\text{Sin}[t])^2+(\text{Cos}[t])^2\right)^{\frac{1}{2}}\right)\Big/$$
$$\left(\left(\epsilon^2*(\text{Cos}[s]-\text{Cos}[t])^2+(\text{Sin}[s]-\text{Sin}[t])^2\right)*\left(\epsilon^2*(\text{Sin}[s])^2+(\text{Cos}[s])^2\right)^{\frac{1}{2}}\right)$$

$$\frac{\left(\epsilon\,\text{Cos}[s]\,(\text{Cos}[s]-\text{Cos}[t])+\epsilon\,\text{Sin}[s]\,(\text{Sin}[s]-\text{Sin}[t])\right)\sqrt{\text{Cos}[t]^2+\epsilon^2\,\text{Sin}[t]^2}}{\sqrt{\text{Cos}[s]^2+\epsilon^2\,\text{Sin}[s]^2}\,\left(\epsilon^2\,(\text{Cos}[s]-\text{Cos}[t])^2+(\text{Sin}[s]-\text{Sin}[t])^2\right)}$$

$$\text{Simplify}\left[\frac{\left(\epsilon\,\text{Cos}[s]\,(\text{Cos}[s]-\text{Cos}[t])+\epsilon\,\text{Sin}[s]\,(\text{Sin}[s]-\text{Sin}[t])\right)\sqrt{\text{Cos}[t]^2+\epsilon^2\,\text{Sin}[t]^2}}{\sqrt{\text{Cos}[s]^2+\epsilon^2\,\text{Sin}[s]^2}\,\left(\epsilon^2\,(\text{Cos}[s]-\text{Cos}[t])^2+(\text{Sin}[s]-\text{Sin}[t])^2\right)}\right]$$

$$-\frac{\epsilon\,\sqrt{1+\epsilon^2-\left(-1+\epsilon^2\right)\text{Cos}[2\,t]}}{\sqrt{2}\,\left(-1-\epsilon^2+\left(-1+\epsilon^2\right)\text{Cos}[s+t]\right)\sqrt{\text{Cos}[s]^2+\epsilon^2\,\text{Sin}[s]^2}}$$

```
-------------------------- Inner Asymptotic Expansion
---------------------------------
```

$$\text{Series}\left[-\frac{\epsilon \sqrt{1+\epsilon^2 - \left(-1+\epsilon^2\right) \text{Cos}[2 \,(\epsilon * T + \pi - s)]}}{\sqrt{2}\,\left(-1-\epsilon^2 + \left(-1+\epsilon^2\right)\text{Cos}[\epsilon * T + \pi]\right)\sqrt{\text{Cos}[s]^2 + \epsilon^2 * \text{Sin}[s]^2}}\,,\,\{\epsilon,\,0,\,3\}\right]$$

$$\frac{\sqrt{2}\,\sqrt{1+\text{Cos}[2\,s]}}{\left(4+T^2\right)\sqrt{\text{Cos}[s]^2}\,\epsilon} + \frac{\sqrt{2}\,T\,\text{Sin}[2\,s]}{\left(4+T^2\right)\sqrt{\text{Cos}[s]^2}\,\sqrt{1+\text{Cos}[2\,s]}} +$$

$$\frac{1}{\sqrt{2}}\left(-\frac{1}{\sqrt{\text{Cos}[s]^2}}\left(\frac{\left(-12\,T^2 - T^4\right)\sqrt{1+\text{Cos}[2\,s]}}{6\left(4+T^2\right)^2} - \left(-1+2\,T^2\,\text{Cos}[2\,s] + \text{Cos}[2\,s]^2 + 2\,T^2\,\text{Cos}[2\,s]^2 + \right.\right.\right.$$

$$\left.\left.\left.T^2\,\text{Sin}[2\,s]^2\right)\middle/\left(2\left(-2-\frac{T^2}{2}\right)(1+\text{Cos}[2\,s])^{3/2}\right)\right) + \frac{\sqrt{1+\text{Cos}[2\,s]}\,\text{Tan}[s]^2}{2\left(-2-\frac{T^2}{2}\right)\sqrt{\text{Cos}[s]^2}}\right)\epsilon +$$

$$\frac{1}{\sqrt{2}}\left(-\frac{1}{\sqrt{\text{Cos}[s]^2}}\left(\frac{T\left(-12\,T^2 - T^4\right)\text{Sin}[2\,s]}{6\left(4+T^2\right)^2\sqrt{1+\text{Cos}[2\,s]}} + \left(-9\,T\,\text{Sin}[2\,s] - 4\,T^3\,\text{Sin}[2\,s] - \right.\right.\right.$$

$$12\,T\,\text{Cos}[2\,s]\,\text{Sin}[2\,s] - 2\,T^3\,\text{Cos}[2\,s]\,\text{Sin}[2\,s] - 3\,T\,\text{Cos}[2\,s]^2\,\text{Sin}[2\,s] +$$

$$\left.\left.2\,T^3\,\text{Cos}[2\,s]^2\,\text{Sin}[2\,s] + 3\,T^3\,\text{Sin}[2\,s]^3\right)\middle/\left(6\left(-2-\frac{T^2}{2}\right)(1+\text{Cos}[2\,s])^{5/2}\right)\right) +$$

$$\left.\frac{T\,\text{Sin}[2\,s]\,\text{Tan}[s]^2}{2\left(-2-\frac{T^2}{2}\right)\sqrt{\text{Cos}[s]^2}\,\sqrt{1+\text{Cos}[2\,s]}}\right)\epsilon^2 + \frac{1}{\sqrt{2}}$$

$$\left(-\frac{1}{\sqrt{\text{Cos}[s]^2}}\left(\frac{\left(-480\,T^4 - 52\,T^6 - 3\,T^8\right)\sqrt{1+\text{Cos}[2\,s]}}{360\left(4+T^2\right)^3} - \right.\right.$$

$$\left(\left(-12\,T^2 - T^4\right)\left(-1+2\,T^2\,\text{Cos}[2\,s] + \text{Cos}[2\,s]^2 + 2\,T^2\,\text{Cos}[2\,s]^2 + T^2\,\text{Sin}[2\,s]^2\right)\right)\middle/$$

$$\left(12\left(4+T^2\right)^2(1+\text{Cos}[2\,s])^{3/2}\right) - \left(3 - 36\,T^2\,\text{Cos}[2\,s] - 8\,T^4\,\text{Cos}[2\,s] - 6\,\text{Cos}[2\,s]^2 - \right.$$

$$84\,T^2\,\text{Cos}[2\,s]^2 - 12\,T^4\,\text{Cos}[2\,s]^2 - 60\,T^2\,\text{Cos}[2\,s]^3 + 3\,\text{Cos}[2\,s]^4 - 12\,T^2\,\text{Cos}[2\,s]^4 +$$

$$4\,T^4\,\text{Cos}[2\,s]^4 - 42\,T^2\,\text{Sin}[2\,s]^2 - 16\,T^4\,\text{Sin}[2\,s]^2 - 48\,T^2\,\text{Cos}[2\,s]\,\text{Sin}[2\,s]^2 +$$

$$4\,T^4\,\text{Cos}[2\,s]\,\text{Sin}[2\,s]^2 - 6\,T^2\,\text{Cos}[2\,s]^2\,\text{Sin}[2\,s]^2 + 20\,T^4\,\text{Cos}[2\,s]^2\,\text{Sin}[2\,s]^2 +$$

$$\left.15\,T^4\,\text{Sin}[2\,s]^4\right)\middle/\left(24\left(-2-\frac{T^2}{2}\right)(1+\text{Cos}[2\,s])^{7/2}\right)\right) + \frac{1}{2\sqrt{\text{Cos}[s]^2}}$$

$$\left(\frac{\left(-12\,T^2 - T^4\right)\sqrt{1+\text{Cos}[2\,s]}}{6\left(4+T^2\right)^2} - \left(-1+2\,T^2\,\text{Cos}[2\,s] + \text{Cos}[2\,s]^2 + 2\,T^2\,\text{Cos}[2\,s]^2 + T^2\,\text{Sin}[2\,s]^2\right)\middle/\right.$$

$$\left.\left.\left(2\left(-2-\frac{T^2}{2}\right)(1+\text{Cos}[2\,s])^{3/2}\right)\right)\text{Tan}[s]^2 - \frac{3\sqrt{1+\text{Cos}[2\,s]}\,\text{Tan}[s]^4}{8\left(-2-\frac{T^2}{2}\right)\sqrt{\text{Cos}[s]^2}}\right)\epsilon^3 + O[\epsilon]^4$$

$$\frac{1}{2*\pi} * \text{Integrate}\Big[$$

$$\left(\frac{\sqrt{2}\,\sqrt{1+\text{Cos}[2\,s]}}{\left(4+T^2\right)\sqrt{\text{Cos}[s]^2}\,\epsilon} + \frac{\sqrt{2}\,T\,\text{Sin}[2\,s]}{\left(4+T^2\right)\sqrt{\text{Cos}[s]^2}\,\sqrt{1+\text{Cos}[2\,s]}}\right) * (\mu[\pi-s]) * \epsilon,\,\left\{T,\,-\frac{\delta}{\epsilon},\,\frac{\delta}{\epsilon}\right\}\Big]$$

$$\text{ConditionalExpression}\left[\frac{\text{ArcTan}\left[\frac{\delta}{2\,\epsilon}\right]\mu[\pi-s]}{\pi},\,\text{Re}\left[\frac{\epsilon}{\delta}\right]\neq 0\,||\,\text{Im}\left[\frac{\epsilon}{\delta}\right] > \frac{1}{2}\,||\,\text{Im}\left[\frac{\epsilon}{\delta}\right] < -\frac{1}{2}\right]$$

$$\frac{1}{2*\pi}*\text{Integrate}\left[\left(\frac{\sqrt{2}\ \sqrt{1+\text{Cos}[2\,s]}}{\left(4+T^2\right)\ \sqrt{\text{Cos}[s]^2}\ \epsilon}\right)*(\mu[\pi-s])*\epsilon,\ \left\{T,\ -\frac{\delta}{\epsilon},\ \frac{\delta}{\epsilon}\right\}\right]$$

$$\text{ConditionalExpression}\left[\frac{\text{ArcTan}\left[\frac{\delta}{2\,\epsilon}\right]\ \mu[\pi-s]}{\pi},\ \text{Re}\left[\frac{\epsilon}{\delta}\right]\neq0\ ||\ \text{Im}\left[\frac{\epsilon}{\delta}\right]>\frac{1}{2}\ ||\ \text{Im}\left[\frac{\epsilon}{\delta}\right]<-\frac{1}{2}\right]$$

$$\frac{1}{2*\pi}*\text{Integrate}\left[\left(\frac{\sqrt{2}\ T\,\text{Sin}[2\,s]}{\left(4+T^2\right)\ \sqrt{\text{Cos}[s]^2}\ \sqrt{1+\text{Cos}[2\,s]}}\right)*(\mu[\pi-s])*\epsilon,\ \left\{T,\ -\frac{\delta}{\epsilon},\ \frac{\delta}{\epsilon}\right\}\right]$$

0

Appendix E

Exterior Helmholtz Inner Asymptotic Expansion

After analyzing the kernel we know that the parts of the kernel that need a correction are L1 and L2 for when i ≠ j.

------------------------------------- L1when i ≠ j --

We start with the inner asymptotic expansion for L1

We start by simplifying the kernel

In[219]:= `Simplify[(ϵ * Cos[s] - ϵ * Cos[t])² + (Sin[s] - Sin[t])²]`

Out[219]= $(\epsilon\, \text{Cos}[s] - \epsilon\, \text{Cos}[t])^2 + (\text{Sin}[s] - \text{Sin}[t])^2$

In[220]:= `TrigReduce[(ϵ Cos[s] - ϵ Cos[t])² + (Sin[s] - Sin[t])²]`

Out[220]= $\frac{1}{2} \left(2 + 2\,\epsilon^2 - \text{Cos}[2\,s] + \epsilon^2\,\text{Cos}[2\,s] - 2\,\text{Cos}[s - t] - \right.$
$\left. 2\,\epsilon^2\,\text{Cos}[s - t] - \text{Cos}[2\,t] + \epsilon^2\,\text{Cos}[2\,t] + 2\,\text{Cos}[s + t] - 2\,\epsilon^2\,\text{Cos}[s + t]\right)$

In[227]:= `Simplify[`$\frac{1}{2}$ `(2 + 2 ϵ² - Cos[2 s] + ϵ² Cos[2 s] - 2 Cos[s - t] -`
$2\,\epsilon^2\,\text{Cos}[s - t] - \text{Cos}[2\,t] + \epsilon^2\,\text{Cos}[2\,t] + 2\,\text{Cos}[s + t] - 2\,\epsilon^2\,\text{Cos}[s + t])]$

Out[227]= $-2\left(-1 - \epsilon^2 + (-1 + \epsilon^2)\,\text{Cos}[s + t]\right)\text{Sin}\left[\frac{s - t}{2}\right]^2$

In[235]:=

$\text{Simplify}\left[\dfrac{k\,\epsilon\,(-1 + \text{Cos}[s - t])}{2\sqrt{2}\,\pi\sqrt{-(-1 - \epsilon^2 + (-1 + \epsilon^2)\,\text{Cos}[s + t])\,\text{Sin}\left[\frac{s-t}{2}\right]^2}} * \right.$

$\left. \text{BesselJ}\left[1, k\sqrt{-2(-1 - \epsilon^2 + (-1 + \epsilon^2)\,\text{Cos}[s + t])\,\text{Sin}\left[\frac{s-t}{2}\right]^2}\right]\right]$

Out[235]= $\dfrac{k\,\epsilon\,\text{BesselJ}\left[1, \sqrt{2}\,k\sqrt{-(-1 - \epsilon^2 + (-1 + \epsilon^2)\,\text{Cos}[s + t])\,\text{Sin}\left[\frac{s-t}{2}\right]^2}\,\right](-1 + \text{Cos}[s - t])}{2\sqrt{2}\,\pi\sqrt{(1 + \epsilon^2 - (-1 + \epsilon^2)\,\text{Cos}[s + t])\,\text{Sin}\left[\frac{s-t}{2}\right]^2}}$

We now do a series expansion

In[270]:= `Assuming[ε > 0 && δ > 0, {Series[`

$$\left(k \text{ } \epsilon \text{ BesselJ}\left[1, k \sqrt{\epsilon^2 (\text{Cos}[s] - \text{Cos}[\pi + \epsilon * T - s])^2 + (\text{Sin}[s] - \text{Sin}[\pi + \epsilon * T - s])^2}\right] \right.$$

$$\left. \text{Sin}\left[\frac{s - (\pi + \epsilon * T - s)}{2}\right]^2 \right) \Big/$$

$$\left(2 \sqrt{2} \text{ } \pi \sqrt{-(-1 - \epsilon^2 + (-1 + \epsilon^2) \text{Cos}[\pi + \epsilon * T]) \text{ Sin}\left[\frac{s - (\pi + \epsilon * T - s)}{2}\right]^2} \right), \{\epsilon, 0, 3\}]\}]$

Out[270]= $\left\{ \left(-\dfrac{\sqrt{4 + T^2}}{k (-24 \text{ Cos}[s] - 6 T^2 \text{ Cos}[s])} \right)^{\text{Floor}\left[\frac{\text{Arg}\left[\frac{k\left(-4\epsilon\text{Cos}[s] - T^2\epsilon\text{Cos}[s] + \sqrt{4+T^2}\sqrt{\epsilon^2(\text{Cos}[s]+\text{Cos}[s-T\epsilon])^2+(\text{Sin}[s]-\text{Sin}[s-T\epsilon])^2}}{\sqrt{4+T^2}}\right]}{2\pi}\right]} \right.$

$$\left(-\dfrac{k (-24 \text{ Cos}[s] - 6 T^2 \text{ Cos}[s])}{\sqrt{4 + T^2}} \right)^{\text{Floor}\left[\frac{\text{Arg}\left[\frac{k\left(-4\epsilon\text{Cos}[s] - T^2\epsilon\text{Cos}[s] + \sqrt{4+T^2}\sqrt{\epsilon^2(\text{Cos}[s]+\text{Cos}[s-T\epsilon])^2+(\text{Sin}[s]-\text{Sin}[s-T\epsilon])^2}}{\sqrt{4+T^2}}\right]}{2\pi}\right]}$$

$$\left(\frac{k^2 \text{ Cos}[s]^2 \text{ } \epsilon}{4 \pi} + \frac{k^2 \text{ } T \text{ Cos}[s] \text{ Sin}[s] \text{ } \epsilon^2}{4 \pi} + \frac{1}{32 \pi} \right.$$

$$\left. \left. (-2 k^2 T^2 \text{ Cos}[s]^2 - 4 k^4 \text{ Cos}[s]^4 - k^4 T^2 \text{ Cos}[s]^4 + 2 k^2 T^2 \text{ Sin}[s]^2) \text{ } \epsilon^3 + O[\epsilon]^4 \right) \right\}$$

We now integrate taking leading order terms

In[271]:= `Assuming[ε > 0 && δ > 0,`

$$\left\{ \text{Integrate}\left[\left(-\frac{\sqrt{4 + T^2}}{k (-24 \text{ Cos}[s] - 6 T^2 \text{ Cos}[s])} \right)^{\text{Floor}\left[\frac{\text{Arg}\left[\frac{k\left(-4\text{Cos}[s]\epsilon - T^2\epsilon\text{Cos}[s] + \sqrt{4+T^2}\sqrt{\epsilon^2(\text{Cos}[s]+\text{Cos}[s-T\epsilon])^2+(\text{Sin}[s]-\text{Sin}[s-T\epsilon])^2}}{\sqrt{4+T^2}}\right]}{2\pi}\right]} \right.$$

$$\left(-\frac{k (-24 \text{ Cos}[s] - 6 T^2 \text{ Cos}[s])}{\sqrt{4 + T^2}} \right)^{\text{Floor}\left[\frac{\text{Arg}\left[\frac{k\left(-4\epsilon\text{Cos}[s] - T^2\epsilon\text{Cos}[s] + \sqrt{4+T^2}\sqrt{\epsilon^2(\text{Cos}[s]+\text{Cos}[s-T\epsilon])^2+(\text{Sin}[s]-\text{Sin}[s-T\epsilon])^2}}{\sqrt{4+T^2}}\right]}{2\pi}\right]} *$$

$$\left. \frac{k^2 \text{ Cos}[s]^2 \text{ } \epsilon}{4 \pi} * (\mu [\pi - s]) * \epsilon, \left\{T, -\frac{\delta}{\epsilon}, \frac{\delta}{\epsilon}\right\}\right]\right\}]$$

Out[271]= $\left\{ \dfrac{k^2 \text{ } \delta \text{ } \epsilon \text{ Cos}[s]^2 \text{ } \mu [\pi - s]}{2 \pi} \right\}$

-- L2 when i ≠ j --

Expanding L2

We start by simplifying the kernel

In[262]:= $\text{Simplify}\Big[\dfrac{\mathbb{i}\, k\, \epsilon\, \text{Sin}\big[\frac{s-t}{2}\big]^2}{\sqrt{2}\,\sqrt{-\big(-1-\epsilon^2+(-1+\epsilon^2)\,\text{Cos}[s+t]\big)\,\text{Sin}\big[\frac{s-t}{2}\big]^2}}\, *$

$\text{HankelH1}\Big[1,\, k*\big(\epsilon^2\,(\text{Cos}[s]-\text{Cos}[t])^2+(\text{Sin}[s]-\text{Sin}[t])^2\big)^{\frac{1}{2}}\Big]\Big]$

Out[262]= $\Big(\mathbb{i}\, k\, \epsilon\, \text{HankelH1}\Big[1,\, k\,\sqrt{\epsilon^2\,(\text{Cos}[s]-\text{Cos}[t])^2+(\text{Sin}[s]-\text{Sin}[t])^2}\,\Big]\,\text{Sin}\big[\frac{s-t}{2}\big]^2\Big)\Big/$

$\Big(\sqrt{2}\,\sqrt{\big(1+\epsilon^2-(-1+\epsilon^2)\,\text{Cos}[s+t]\big)\,\text{Sin}\big[\frac{s-t}{2}\big]^2}\,\Big)$

In[263]:= $\text{TrigReduce}\Big[$

$\Big(\mathbb{i}\, k\, \epsilon\, \text{HankelH1}\Big[1,\, k\,\sqrt{\epsilon^2\,(\text{Cos}[s]-\text{Cos}[t])^2+(\text{Sin}[s]-\text{Sin}[t])^2}\,\Big]\,\text{Sin}\big[\frac{s-t}{2}\big]^2\Big)\Big/$

$\Big(\sqrt{2}\,\sqrt{\big(1+\epsilon^2-(-1+\epsilon^2)\,\text{Cos}[s+t]\big)\,\text{Sin}\big[\frac{s-t}{2}\big]^2}\,\Big)\Big]$

Out[263]= $-\Big(\Big(\mathbb{i}\,\Big(-k\,\epsilon\,\text{HankelH1}\Big[1,\, k\,\sqrt{\epsilon^2\,(\text{Cos}[s]-\text{Cos}[t])^2+(\text{Sin}[s]-\text{Sin}[t])^2}\,\Big]+$

$k\,\epsilon\,\text{Cos}[s-t]\,\text{HankelH1}\Big[1,\, k\,\sqrt{\epsilon^2\,(\text{Cos}[s]-\text{Cos}[t])^2+(\text{Sin}[s]-\text{Sin}[t])^2}\,\Big]\Big)\Big)\Big/$

$\Big(2\,\sqrt{2}\,\sqrt{-\big(-1-\epsilon^2-\text{Cos}[s+t]+\epsilon^2\,\text{Cos}[s+t]\big)\,\text{Sin}\big[\frac{s}{2}-\frac{t}{2}\big]^2}\,\Big)\Big)$

In[264]:= $\text{Simplify}[\%263]$

Out[264]= $\Big(\mathbb{i}\, k\, \epsilon\, \text{HankelH1}\Big[1,\, k\,\sqrt{\epsilon^2\,(\text{Cos}[s]-\text{Cos}[t])^2+(\text{Sin}[s]-\text{Sin}[t])^2}\,\Big]\,\text{Sin}\big[\frac{s-t}{2}\big]^2\Big)\Big/$

$\Big(\sqrt{2}\,\sqrt{-\big(-1-\epsilon^2+(-1+\epsilon^2)\,\text{Cos}[s+t]\big)\,\text{Sin}\big[\frac{s-t}{2}\big]^2}\,\Big)$

We now do a series expansion

In[268]:= $\text{Assuming}\Big[\epsilon>0\,\&\&\,\delta>0,\,\Big\{\text{Series}\Big[$

$\Big(\mathbb{i}\, k\, \epsilon\, \text{HankelH1}\Big[1,\, k\,\sqrt{\big(\epsilon^2\,(\text{Cos}[s]-\text{Cos}[\pi+\epsilon*T-s])^2+(\text{Sin}[s]-\text{Sin}[\pi+\epsilon*T-s])^2\big)}\,\Big]$

$\text{Sin}\big[\frac{s-(\pi+\epsilon*T-s)}{2}\big]^2\Big)\Big/$

$\Big(\sqrt{2}\,\sqrt{\big(-(-1-\epsilon^2+(-1+\epsilon^2)\,\text{Cos}[\pi+\epsilon*T])\big)\,\text{Sin}\big[\frac{s-(\pi+\epsilon*T-s)}{2}\big]^2}\,\Big)\Big),\,\{\epsilon,0,3\}\Big]\Big\}\Big]$

Out[268]= $\Big\{\Big(\dfrac{2}{\pi\,(4+T^2)\,\epsilon}+\dfrac{1}{6\,\pi\,(4+T^2)^{5/2}}$

$\Big(12\,T^2\,\sqrt{4+T^2}+T^4\,\sqrt{4+T^2}+368\,k^2\,\sqrt{4+T^2}\,\text{Cos}[s]^2-96\,\text{EulerGamma}\,k^2\,\sqrt{4+T^2}\,\text{Cos}[s]^2+$

$$184 k^2 T^2 \sqrt{4+T^2} \, Cos[s]^2 - 48 \, EulerGamma \, k^2 T^2 \sqrt{4+T^2} \, Cos[s]^2 +$$

$$23 k^2 T^4 \sqrt{4+T^2} \, Cos[s]^2 - 6 \, EulerGamma \, k^2 T^4 \sqrt{4+T^2} \, Cos[s]^2 -$$

$$320 k^2 \, Cos[s] \sqrt{(4+T^2) \, Cos[s]^2} - 160 k^2 T^2 \, Cos[s] \sqrt{(4+T^2) \, Cos[s]^2} -$$

$$20 k^2 T^4 \, Cos[s] \sqrt{(4+T^2) \, Cos[s]^2} - 96 k^2 \sqrt{4+T^2} \, Cos[s]^2 \, Log[\epsilon] -$$

$$48 k^2 T^2 \sqrt{4+T^2} \, Cos[s]^2 \, Log[\epsilon] - 6 k^2 T^4 \sqrt{4+T^2} \, Cos[s]^2 \, Log[\epsilon] -$$

$$96 k^2 \sqrt{4+T^2} \, Cos[s]^2 \, Log\Big[- \frac{k \left(-24 \, Cos[s] - 6 T^2 \, Cos[s]\right)}{12 \sqrt{4+T^2}} \Big] -$$

$$48 k^2 T^2 \sqrt{4+T^2} \, Cos[s]^2 \, Log\Big[- \frac{k \left(-24 \, Cos[s] - 6 T^2 \, Cos[s]\right)}{12 \sqrt{4+T^2}} \Big] -$$

$$6 k^2 T^4 \sqrt{4+T^2} \, Cos[s]^2 \, Log\Big[- \frac{k \left(-24 \, Cos[s] - 6 T^2 \, Cos[s]\right)}{12 \sqrt{4+T^2}} \Big] \Big) \epsilon + O[\epsilon]^2 \Big) +$$

$$\left(- \frac{\sqrt{4+T^2}}{k \left(-24 \, Cos[s] - 6 T^2 \, Cos[s]\right)} \right)^{Floor\left[\frac{Arg\left[\frac{k\left(-4\epsilon \, Cos[s] - T^2 \epsilon \, Cos[s] + \sqrt{4+T^2} \sqrt{\epsilon^2 \left(Cos[s] + Cos[s-T\epsilon]\right)^2 + \left(Sin[s] - Sin[s-T\epsilon]\right)^2}\right)}{\sqrt{4+T^2}} \right]}{2\pi} \right]}$$

$$\left(- \frac{k \left(-24 \, Cos[s] - 6 T^2 \, Cos[s]\right)}{\sqrt{4+T^2}} \right)^{Floor\left[\frac{Arg\left[\frac{k\left(-4\epsilon \, Cos[s] - T^2 \epsilon \, Cos[s] + \sqrt{4+T^2} \sqrt{\epsilon^2 \left(Cos[s] + Cos[s-T\epsilon]\right)^2 + \left(Sin[s] - Sin[s-T\epsilon]\right)^2}\right)}{\sqrt{4+T^2}} \right]}{2\pi} \right]}$$

$$\left(\frac{1}{2} \mathbb{i} \, k^2 \, Cos[s]^2 \, \epsilon + \frac{1}{2} \mathbb{i} \, k^2 \, T \, Cos[s] \, Sin[s] \, \epsilon^2 - \right.$$

$$\left. \frac{1}{16} \mathbb{i} \, k^2 \left(2 T^2 \, Cos[s]^2 + 4 k^2 \, Cos[s]^4 + k^2 T^2 \, Cos[s]^4 - 2 T^2 \, Sin[s]^2\right) \epsilon^3 + O[\epsilon]^4 \right) +$$

$$Floor\Big[\frac{1}{2\pi} Arg\Big[\frac{1}{\sqrt{4+T^2}} k \Big(-4 \epsilon \, Cos[s] - T^2 \epsilon \, Cos[s] + $$

$$\sqrt{4+T^2} \sqrt{\left(\epsilon^2 \left(Cos[s] + Cos[s-T\epsilon]\right)^2 + \left(Sin[s] - Sin[s-T\epsilon]\right)^2\right)} \Big) \Big] \Big] \Big]$$

$$\left(- \frac{k^2 \, Cos[s]^2 \, Log\Big[- \frac{12\sqrt{4+T^2}}{k\left(-24 \, Cos[s] - 6 T^2 \, Cos[s]\right)} \Big] \epsilon}{\pi} - \right.$$

$$\frac{k^2 \, T \, Cos[s] \, Log\Big[- \frac{12\sqrt{4+T^2}}{k\left(-24 \, Cos[s] - 6 T^2 \, Cos[s]\right)} \Big] \, Sin[s] \, \epsilon^2}{\pi} +$$

$$\frac{1}{8\pi} Log\Big[- \frac{12\sqrt{4+T^2}}{k\left(-24 \, Cos[s] - 6 T^2 \, Cos[s]\right)} \Big]$$

$$\left. \left(2 k^2 T^2 \, Cos[s]^2 + 4 k^4 \, Cos[s]^4 + k^4 T^2 \, Cos[s]^4 - 2 k^2 T^2 \, Sin[s]^2\right) \epsilon^3 + O[\epsilon]^4 \right) +$$

$$\text{Floor}\Big[\frac{1}{2\pi}\text{Arg}\Big[\frac{1}{\sqrt{4+T^2}}k\Big(-4\,\epsilon\,\text{Cos[s]}-T^2\,\epsilon\,\text{Cos[s]}+$$

$$\sqrt{4+T^2}\,\sqrt{\Big(\epsilon^2\,\big(\text{Cos[s]}+\text{Cos[s}-T\,\epsilon]\big)^2+\big(\text{Sin[s]}-\text{Sin[s}-T\,\epsilon]\big)^2\Big)}\Big)\Big]\Big]$$

$$\Bigg(-\frac{k^2\,\text{Cos[s]}^2\,\text{Log}\Big[-\frac{k\,(-24\,\text{Cos[s]}-6\,T^2\,\text{Cos[s]})}{12\,\sqrt{4+T^2}}\Big]\,\epsilon}{\pi}-$$

$$\frac{k^2\,T\,\text{Cos[s]}\,\text{Log}\Big[-\frac{k\,(-24\,\text{Cos[s]}-6\,T^2\,\text{Cos[s]})}{12\,\sqrt{4+T^2}}\Big]\,\text{Sin[s]}\,\epsilon^2}{\pi}+$$

$$\frac{1}{8\,\pi}\text{Log}\Big[-\frac{k\,\big(-24\,\text{Cos[s]}-6\,T^2\,\text{Cos[s]}\big)}{12\,\sqrt{4+T^2}}\Big]$$

$$\big(2\,k^2\,T^2\,\text{Cos[s]}^2+4\,k^4\,\text{Cos[s]}^4+k^4\,T^2\,\text{Cos[s]}^4-2\,k^2\,T^2\,\text{Sin[s]}^2\big)\,\epsilon^3+O[\epsilon]^4\Bigg)\Bigg\}$$

We now integrate taking leading order terms

In[269]:= $\text{Integrate}\Big[\frac{2}{\pi\,(4+T^2)\,\epsilon}*(\mu[\pi-s])*\epsilon,\,\Big\{T,\,-\frac{\delta}{\epsilon},\,\frac{\delta}{\epsilon}\Big\}\Big]$

Out[269]= $\text{ConditionalExpression}\Big[\frac{2\,\text{ArcTan}\big[\frac{\delta}{2\,\epsilon}\big]\,\mu[\pi-s]}{\pi},\,\text{Re}\big[\frac{\epsilon}{\delta}\big]\neq 0\,||\,\text{Im}\big[\frac{\epsilon}{\delta}\big]>\frac{1}{2}\,||\,\text{Im}\big[\frac{\epsilon}{\delta}\big]<-\frac{1}{2}\Big]$

Appendix F

Asymptotic Matching for the Interior Dirichlet Laplace problem

From previous work we found that the boundary integral equation for a narrow ellipse is

$$-\frac{1}{2}\mu(s) + \frac{1}{2\pi}\int_0^{2\pi} k(s,t;\epsilon)\mu(t)\mathrm{d}t = f(s), \quad 0 \le s \le 2\pi, \tag{F.1}$$

with

$$k(s,t;\epsilon) = \frac{\epsilon}{-1-\epsilon^2-(1-\epsilon^2)\cos(s+t)} \tag{F.2}$$

F.1 Inner Expansion

We first wish to obtain an inner expansion of the integral,

$$I = \frac{1}{2\pi}\int_0^{2\pi} k(s,t;\epsilon)\mu(t)\mathrm{d}t \tag{F.3}$$

such expansion is obtain in a similar way as the inner expansion for the modified trapezoid method one difference is that instead of considering Δt we now introduce a generic parameter δ which satisfies the asymptotic relation, $0 < \epsilon \ll \delta < 1$. We then consider $\delta = \sqrt{\epsilon}$ so that

$$I_{inner}(s,t;\epsilon,\delta) = \frac{1}{2\pi}\int_{\pi-s-\delta}^{\pi-s+\delta} k(s,t;\epsilon)\mu(t)\mathrm{d}t \tag{F.4}$$

In order to calculate the inner expansion we nee d to make some substitutions. First we let

$$t = \tau + \pi - s \tag{F.5}$$

$$\mathrm{d}t = \mathrm{d}\tau \tag{F.6}$$

so that

$$I_{inner} = \frac{1}{2\pi}\int_{-\delta}^{\delta} \frac{\epsilon}{-1-\epsilon^2-(1-\epsilon^2)\cos(\tau+\pi)}\mu(\tau+\pi-s)\mathrm{d}\tau \tag{F.7}$$

Now we let

$$\tau = \epsilon T \tag{F.8}$$

$$\mathrm{d}\tau = \epsilon \mathrm{d}T \tag{F.9}$$

so that

$$I_{inner} = \frac{1}{2\pi} \int_{\frac{-\delta}{\epsilon}}^{\frac{\delta}{\epsilon}} \frac{\epsilon}{-1 - \epsilon^2 - (1 - \epsilon^2)\cos(\epsilon T + \pi)} \mu(\epsilon T + \pi - s)\epsilon \mathrm{d}T \tag{F.10}$$

Expanding to second order ϵ for $\epsilon = 0$,

$$I_{inner} = \frac{1}{2\pi} \int_{\frac{-\delta}{\epsilon}}^{\frac{\delta}{\epsilon}} \left(\frac{1}{\left(-2 - \frac{T^2}{2}\right)\epsilon} + \frac{(-12T^2 - T^4)\epsilon}{6(4 + T^2)^2} \right) (\mu(\pi - s) + \epsilon T \mu'(\pi - s) + \frac{\epsilon^2 T^2}{2}\mu''(\pi - s))\epsilon \mathrm{d}T \tag{F.11}$$

$$= -\frac{\arctan(\frac{\delta}{2\epsilon})\mu(\pi - s)}{\pi} - \frac{\delta^3 \epsilon}{6\pi(\delta^2 + 4\epsilon^2)}\mu(\pi - s) - \frac{\epsilon^2(\frac{2\delta}{\epsilon} - 4\arctan(\frac{\delta}{2\epsilon}))}{2\pi}\mu''(\pi - s) + O(\epsilon^2) \tag{F.12}$$

Expanding for large $\frac{\delta}{\epsilon}$, we find

$$I_{inner} \sim -\frac{1}{2}\mu(\pi - s) + \frac{2\epsilon}{\pi\delta}\mu(\pi - s) - \frac{\epsilon\delta}{6\pi}\mu(\pi - s) + \frac{\delta\epsilon}{\pi}\mu''(\pi - s) - \epsilon^2\mu''(\pi - s) + O(\epsilon^2) \tag{F.13}$$

since $-\epsilon^2\mu''(\pi - s)$ is a second order ϵ term we obtain

$$I_{inner} \sim -\frac{1}{2}\mu(\pi - s) + \frac{2\epsilon}{\pi\delta}\mu(\pi - s) - \frac{\epsilon\delta}{6\pi}\mu(\pi - s) + \frac{\delta\epsilon}{\pi}\mu''(\pi - s) + O(\epsilon^2) \tag{F.14}$$

F.2   Outer Expansion

Next we seek an outer expansion such that

$$I_{outer}(s, t; \epsilon, \delta) = \frac{1}{2\pi} \int_0^{\pi - s + \delta} k(s, t; \epsilon)\mu(t)\mathrm{d}t + \frac{1}{2\pi} \int_{\pi - s + \delta}^{2\pi} k(s, t; \epsilon)\mu(t)\mathrm{d}t \tag{F.15}$$

Expanding k about ϵ,

$$k(s, t; \epsilon) = -\frac{\epsilon}{1 + \cos(s + t)} + O(\epsilon^3) = -\epsilon k_1(s, t) + O(\epsilon^3) \tag{F.16}$$

Replacing k by this expansion,

$$I_{outer}(s, t; \epsilon, \delta) = \frac{1}{2\pi} \int_0^{\pi - s + \delta} \epsilon(-k_1(s, t; \epsilon))\mu(t)\mathrm{d}t + \frac{1}{2\pi} \int_{\pi - s + \delta}^{2\pi} \epsilon(-k_1(s, t; \epsilon))\mu(t)\mathrm{d}t + \dots \tag{F.17}$$

which can be written as

$$I_{outer} = \frac{1}{2\pi} \int_0^{2\pi} \epsilon(-k_1(s, t; \epsilon))\mu(t)\mathrm{d}t + \frac{1}{2\pi} \int_{\pi - s + \delta}^{\pi - s - \delta} \epsilon(-k_1(s, t; \epsilon))\mu(t)\mathrm{d}t + \dots \tag{F.18}$$

Now we compute the leading-order behavior for the second integral in (F.18) so
that

$$I_1(s, t; \epsilon, \delta) = \frac{1}{2\pi} \int_{\pi-s+\delta}^{\pi-s-\delta} \epsilon(-k_1(s, t; \epsilon))\mu(t)\mathrm{d}t \tag{F.19}$$

In order to compute the leading behavior we have to make a few substitutions,
first we let

$$t = \tau + \pi - s \tag{F.20}$$

$$\mathrm{d}t = \mathrm{d}\tau \tag{F.21}$$

we obtain

$$I_1 = \frac{1}{2\pi} \int_{\delta}^{-\delta} -\epsilon \left(\frac{1}{1 + \cos(\tau + \pi)} \right) \mu(\tau + \pi - s)\mathrm{d}\tau \tag{F.22}$$

let

$$\tau = \epsilon T \tag{F.23}$$

$$\mathrm{d}\tau = \epsilon \mathrm{d}T \tag{F.24}$$

we obtain

$$I_1 = \frac{1}{2\pi} \int_{-\frac{\delta}{\epsilon}}^{\frac{\delta}{\epsilon}} \epsilon \left(\frac{1}{1 + \cos(\epsilon T + \pi)} \right) \mu(\epsilon T + \pi - s)\epsilon \mathrm{d}T \tag{F.25}$$

Expanding to second order ϵ about $\epsilon = 0$

$$I_1 = \frac{1}{2\pi} \int_{-\frac{\delta}{\epsilon}}^{\frac{\delta}{\epsilon}} (\frac{2}{T^2\epsilon^2} + \frac{1}{6} + \frac{T^2\epsilon^2}{120})(\mu(\pi - s) + \epsilon T\mu'(\pi - s) + \frac{\epsilon^2 T^2}{2}\mu''(\pi - s) + O(\epsilon^3))\epsilon^2 \mathrm{d}T \tag{F.26}$$

After factoring the outer expansion is

$$I_1 = \frac{1}{2\pi} \int_{\frac{-\delta}{\epsilon}}^{\frac{\delta}{\epsilon}} \left(\frac{2}{T^2}\mu(\pi - s) + \frac{1}{6}\epsilon^2\mu(\pi - s) + \frac{2\epsilon}{T}\mu'(\pi - s) + \epsilon^2\mu''(\pi - s) + O(\epsilon^3) \right) \mathrm{d}T \tag{F.27}$$

When we integrate we notice that

$$I_1 = \int_{\frac{-\delta}{\epsilon}}^{\frac{\delta}{\epsilon}} \frac{2}{T^2}\mu(\pi - s)\mathrm{d}T \to \infty \tag{F.28}$$

thus, we are not able obtain an outer expansion and we are not able to do an
asymptotic matching. For the interior Dirichlet Laplace prooblem we are only
able to obtain an inner asymptotic expansion.

Appendix G

Body-fitted grid for the exterior Neumann problem

In order to estimate the accuracy of the method we seek an exact solution. Contrary to the interior Dirichlet Laplace problem, there is no straight forward source f to provide an exact solution to equation (50). Here we use an exact solution of (3.1) directly. We consider $u_{exact} = \frac{x - x_o}{|x - x_o|^2}$ with $x_o \in D$ as a solution to the exterior Neumann problem to find $f = \frac{\partial u_{exact}}{\partial n_x}$. We create a grid by extending along the normal on the boundary as shown in Figure H.1. We use a body fitted grid to evaluate outside of the ellipse. We use the points to approximate u_{exact} which will give an exact solution and approximate the single-layer potential

$$u(x) = \int_B \left(-\frac{1}{2\pi} \log |x - y| \right) \mu(y) \mathrm{d}y. \tag{G.1}$$
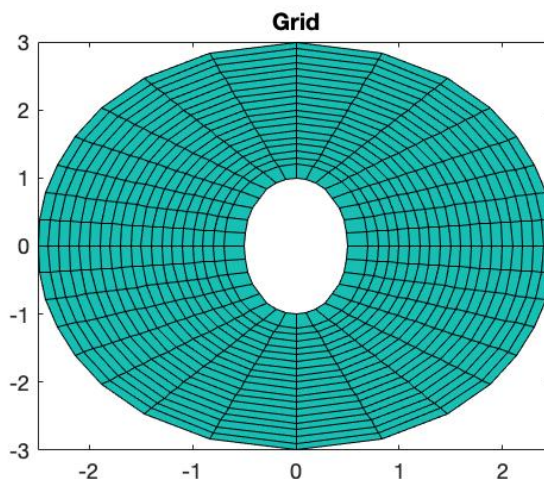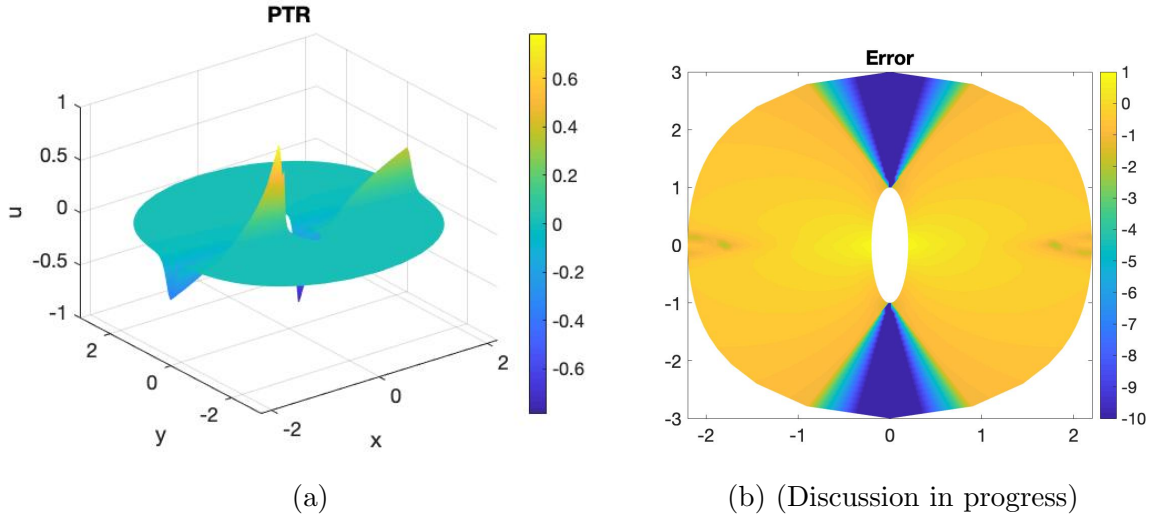

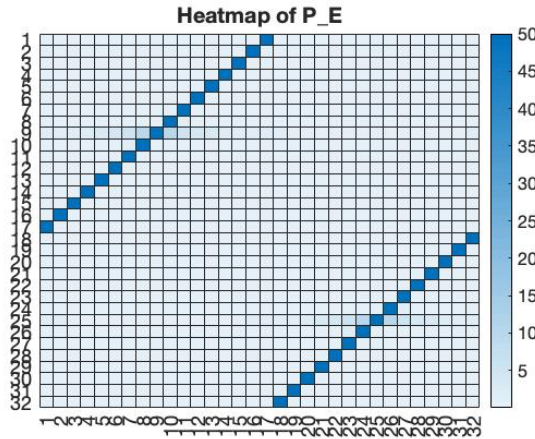Figure G.1: Grid of the ellipse with $\epsilon = 0.5$ and $N = 32$.

Numerical Results

Figure G.2a shows the approximation using PTR. The peaks on the plot correspond to where the kernel is nearly singular $s + t = \pi$ and $s + t = 3\pi$. The diagonals on the heatmap in Figure G.2c correspond to $s + t = \pi$ and $s + t = 3\pi$.

The values along the diagonals are very large this is due to the kernels' behavior at these points. The condition number for matrix P_E is greater than 1, thus the matrix is sensitive to inverse calculation. Recall that we care about the accuracy of the approximation and not so much on computational cost. Figure G.2b shows the log of the absolute error using PTR. The error is large. The regions of high curvature affect our approximation as we see in figure G.2b the error increases as it approximates the regions affected by the curvature of the ellipse.

(a)

(b) (Discussion in progress)

(c) The conditon number of P_E is $1.437235e+00$.

Figure G.2: (a) Periodic Trapezoid Rule approximation of u with $\epsilon = 0.2$ and $N = 64$. (b) plot of the absolute error of the approximation using PTR with $\epsilon = 0.2$ and $N = 64$. (c) Heatmap of the matrix P_E for $\epsilon = 0.01$ and $N = 32$.

Summary

The exterior Neuman problem for a narrow ellipse has a challenging kernel expression. Furthermore, we do not have an exact solution for this problem. We use a body-fitted grid to obtain an approximation of the single-layer potential and obtain a large error. We obtained a large error due to the curvature of our problem and thus conclude that the body fitted grid is not capturing the behavior of our problem. in the regions of high curvature we obtain a large error. A new grid will be implemented that better suits the curvature of our problem.

Appendix H

Body-fitted grid for the exterior Helmholtz problem

In order to estimate the accuracy of the method we seek an exact solution. Similar to the exterior Neumann Laplace problem, there is no straight forward source f to provide an exact solution to equation (89). Here we use an exact solution of (69) directly. The challenge is that we do not have an exact solution for this problem. We consider $u_{exact} = \frac{i}{4} H_0^{(1)}(k|x - x_0|)$ with $x_o \in D$ as a solution to find $f = u_{exact}|_B$. We use the body-fitted grid to evaluate outside of the ellipse and use the points obtained to approximate u_{exact} which will give an exact solution and solve the single- and double- layer potential

$$u(x) = \int_B \left(\frac{\partial G}{\partial n_y}(x, y) - ik G(x, y) \right) \mu(y) \mathrm{d}y. \tag{H.1}$$
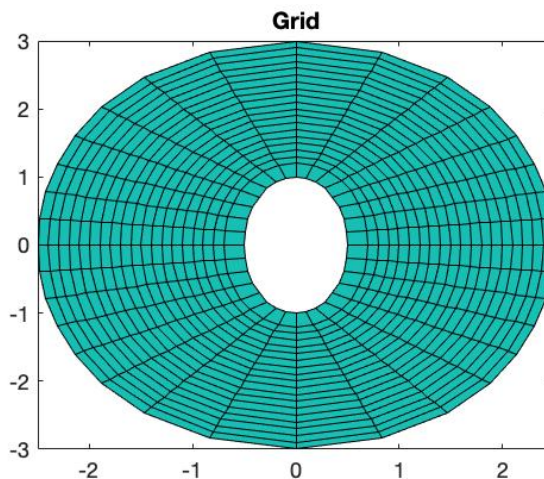

Figure H.1: Grid of the ellipse with $\epsilon = 0.5$ and $N = 32$.

Numerical Results

Figure H.2a is the plot of μ using Kress quadrature. We no longer have a singularity. Figure H.2b is a heatmap of the matrix H, we have big values along the diagonals which correspond to where the kernel is nealy singular $s + t = \pi$ and $s + t = 3\pi$. Figure H.2c correspond to a log surface plot of the error there are

parts where the error is large along our grid of the boundary. A correction needs to be made so that we can improve the approximation.
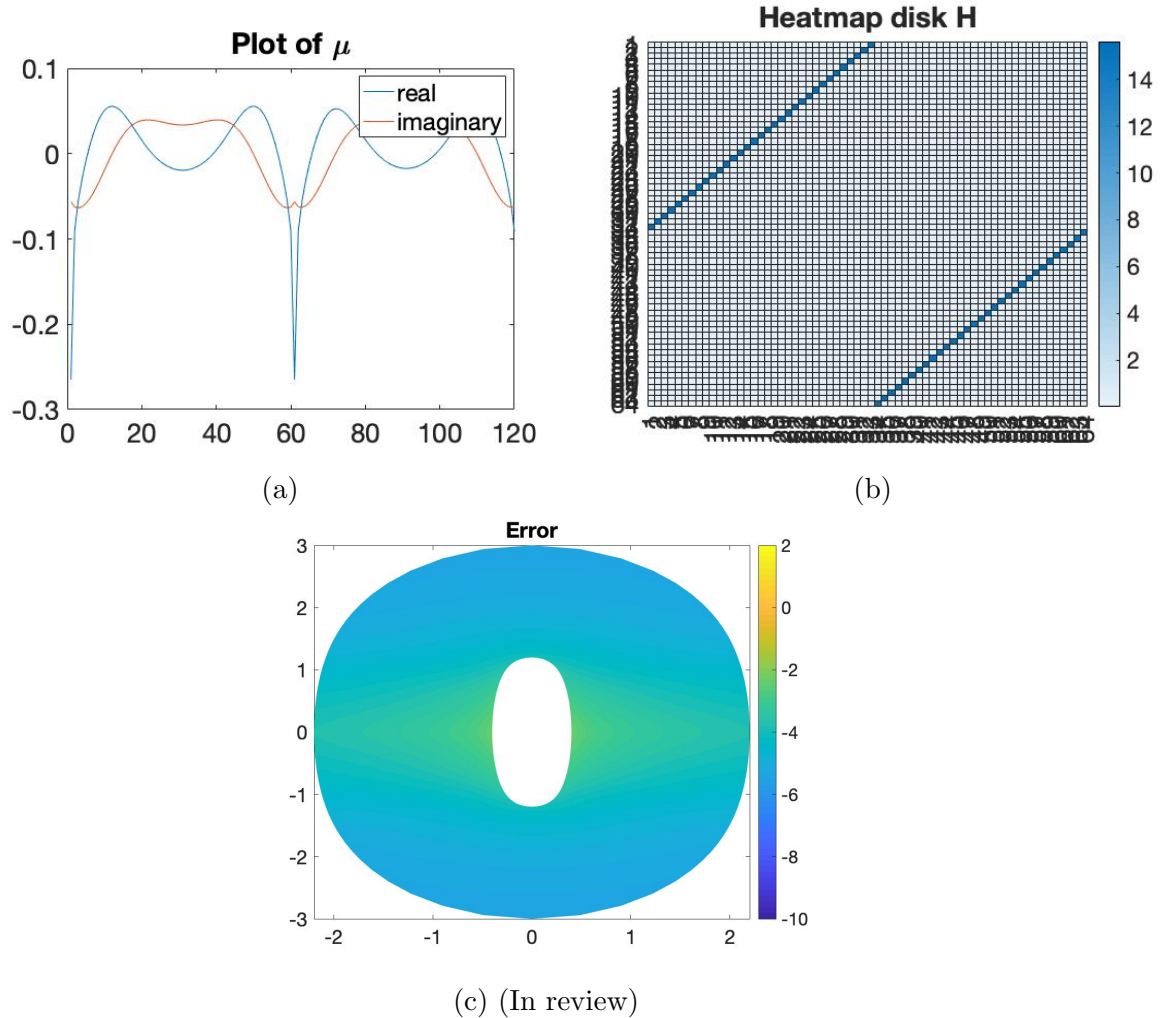

(a)

(b)

(c) (In review)

Figure H.2: (a) Exterior Helmholtz approximation of μ with $\epsilon = 0.001$, $N = 120$ and $k = 5$. (b) Heatmap of matrix H with $\epsilon = 0.001$, $N = 64$ and $k = 5$. (c) The log of the error using $\epsilon = 0.2$, $N = 128$ and $k = 5$.

Summary
The BIE of the exterior Helmholtz problem has a weakly singular integral which makes the problem challenging. Since the kernel of the exterior Helmholtz problem is singular PTR does not work. The Hankel function of the first kind has a log singularity thus we use Kress quadrature to obtain an approximation of the double- and single- layer potential. We obtained a large error due to the curvature of our problem and thus conclude that the body fitted grid is not capturing the behavior of our problem. in the regions of high curvature we obtain a large error. Anew grid will be implemented that better suits the curvature of our problem.

Bibliography

[1] K. Atkinson, *The Numerical Solution of Integral Equations of the Second Kind*, Cambridge University Press, Cambridge, UK, (1997).

[2] J. T. Beale and M.-C. Lai *A method for computing nearly singular integrals* SIAM J. Numer. Anal., 38 (2001), 1902–1925.

[3] J. Beale, W. Ying & J. Wilson. *A Simple Method for Computing Singular or Nearly Singular Integrals on Closed Surfaces.* Communications in Computational Physics. 20 (2016) 733-753.

[4] F. Cakoni & D. Colton. *Qualitative methods in inverse scattering theory: An introduction.* (2006).

[5] C. Carvalho, S. Khatri, A. Kim. *Asymptotic analysis for close evaluation of layer potentials.* Journal of Computational Physics, Elsevier, 355 (2018): 327-341.

[6] C. Carvalho, S. Khatri, A. Kim.*Asymptotic approximations for the close evaluation of double-layer potentials.* SIAM Journal on Scientific Computing 42.1 (2020) A504-A533.

[7] H. Cheng and L. Greengard, *On the numerical evaluation of electrostatic fields in dense random dispersions of cylinders*, J. Comput. Phys.136 (1997), 629–639.

[8] D. Colton and K. Rainer. *Inverse Acoustic and Electromagnetic Scattering Theory.* (1992).

[9] T. A. Cruse *Application of the Boundary-Integral Eq. Method to 3-D Stress Analysis* J. Comp. Strucf. 3, 509-527, Pergamon Press, Oxford (1973).

[10] K. Diethelm *Peano kernels and bounds for the error constants of Gaussian and related quadrature rules for Cauchy principal value integrals.*Numer Math, 73. (1) (1996), 53-63.

[11] U. Frisch, H. Frisch, *Non-LTE transfer – III. Asymptotic expansion for small ϵ*, Monthly Notices of the Royal Astronomical Society, Volume 181, Issue 2, November 1977, 273–280.

[12] J.F. Geer *Rational Trigonometric Approximations Using Fourier Series Partial Sums.* Journal of Scientific Computing. 10 (1995), 325-333.

[13] R. B. Guenther, and J. W. Lee. *Partial Differential Equations of Mathematical Physics and Integral Equations.* Dover Publications, (2014).

[14] J. Helsing, R. Ojala *On the evaluation of layer potentials close to their sources* Journal of Computational Physics, 227 (2008), 2899-2921.

[15] G. C. Hsiao, R. E. Kleinman, and D-Q. Wang. *Applications of boundary integral equation methods in 3D electromagnetic scattering"* Journal of computational and applied mathematics 104.2 (1999): 89-110.

[16] R. Kress. *A Nyström method for boundary integral equations in domains with corners.* Numer. Math., 58 (1990) 145–161.

[17] R. Kress *Boundary integral equations in time-harmonic caustic scattering* Math. Comput. Model.15 (1991) 229-243.

[18] T. Kress, *Linear Integral Equations*, Springer-Verlag, New York, NY, (1999).

[19] U. Lamp, K. Schleicher & W.L. Wendland *The fast Fourier transform and the numerical solution of one-dimensional boundary integral equations.* Numer. Math. 47, 15–38 (1985).

[20] S. S. Lee and R. A. Westmann, *Application of high-order quadrature rules to time-domain boundary element analysis of viscoelasticity.* Int. J. Numer. Meth. Engng., 38(1995), 607-629.

[21] R McGorty, et al. *Measuring dynamics and interactions of colloidal particles with digital holographic microscopy.* Digital Holography and Three-Dimensional Imaging. Optical Society of America, (2008).

[22] W. McLean, *Strongly elliptic systems and boundary integral equations.*(2002).

[23] L. Morino, *Boundary integral equations in aerodynamics.* (1993): 445-466.

[24] M. Ruiz, O. Schnitzer, *Slender-body theory for plasmonic resonance.* Proc. R. Soc. A 475: 20190294 (2019).

[25] V. Sladek, J. Sladek, S. Atluri, *Numerical integration of singularities in meshless implementation of local boundary integral equations.* Computational Mechanics 25 (2000) 394–403.

[26] T. Yang, *Nyström Method vs Random Fourier Features: A Theoretical and Empirical Comparison.* NIPS (2012).

[27] A. Zinchenko, M. Rother,& R. DAVIS, *Cusping, capture, and breakup of interacting drops by a curvatureless boundary-integral algorithm.* Journal of Fluid Mechanics (1999) 249-292.